國立交通大學

光電工程研究所

碩士論文

8-11 keV 穿透式 X 光顯微鏡系統中 Zone plate 傾斜之研究

Zone plate tilt study in transmission X-ray microscope system at 8-11 keV

學生:趙芙涵

指導教授：祁甦, 賴暎杰

8-11 keV 穿透式 X 光顯微鏡系統中 Zone plate 傾斜之研究

學生:趙芙涵　　指導教授：祁甦
賴暎杰

國立交通大學光電工程研究所碩士班

摘要

光學元件 Zone plate 在近幾年來被應用為穿透式 X 光顯微鏡(TXM)系統中的聚焦透鏡。當系統中的 zone plate 被傾斜時,顯微鏡影像會受到像差的影響。以入射光的觀點來看,zone plate 的穿透函數形狀因傾斜改變了,因此傾斜的 zone plate 不再能正常的聚焦入射光。

在本篇論文中,將呈現實驗與模擬的結果。在 TXM 系統中有一個五軸座台可幫助完成此實驗,該座台可以三維的移動 zone plate,以及傾斜 zone plate(以垂直或水平方向為旋轉軸皆可)。根據富立葉光學理論,只要知道光源的光場,每個元件之間的距離,樣品與 zone plate 的穿透函數,即可計算整個顯微鏡系統中任何地方的光場。在此論文中,將運用 matlab 平行處理的程式去完成複雜的計算。以模擬出來的影像和實驗結果做比對,找出顯微鏡影像可接受的 zone plate 最大傾斜角度。

Zone plate tilt study in transmission X-ray microscope system at 8-11 keV

Student: Fu-Han Chao Advisors: Prof. Sien Chi
Prof. Yin-Chieh Lai

The Institute of Electro-Optical Engineering
National Chiao Tung University

ABSTRACT

Zone plate has been used as a focal lens in transmission X-ray microscope (TXM) optical system in recent decades. When zone plate is tilted, the image quality will be affected by aberration. Since for incident beam the shape of zone plate's transmission function will look different when zone plate is tilted, the tilted zone plate cannot focus light normally.

The both experimental and simulation result will be shown in this thesis. A five axes stage is designed and manufactured for the zone plate holder for three dimensional movement, tip and tilt. According to Fourier theory, the wave distribution on image plane can be calculated, if we know the original wave function, the distances between each element, and the transparencies of the sample and zone plate. A parallel simulation process code in MATLAB is developed in workstation cluster with up to 128Gbytes memory. The effects of aberration generated by tilt effect are compared from the experimental data and simulation result. A maximum tilt angle within the acceptable image quality is calculated by simulation and will be verified by experiment.

Acknowledgements

This work is done with the help and collaboration of many people. First, I thank Prof. Sien Chi (祁甦老師) and Prof. Yin Chieh Lai (賴暎杰老師), my advisers in National Chiao Tung University. They gave me some helpful suggestions during these two years of my master research. I thank Prof. Keng Liang (梁耕三老師), the director of NSRRC, who supported the research of zone plate tilt in TXM system, and Prof. Fu-Rong Chen (陳福榮老師), who has discussed about the microscope, Fourier optics and the optical aberration with me.

Thanks for Dr. Gung-Chian Yin (殷廣鈐博士), who installed the TXM system in NSRRC. He taught me how to do experiment in the end station and enlightened me on the problem of zone plate aberration in TXM system. Thanks for Mr. Yu-Tung Chen (陳語同) who fabricated high aspect ratio zone plates and Siemens stars which were used in TXM system. Thanks for Mr. Ping-Chen Tseng (曾斌誠), who help me to learn Matlab and gave me some suggestions. I thank Mr. Ying-Shuo Tseng (曾英碩), Mr. Sin-Yu Lin (林信余), Mr. Kuo Hung Lo (羅國宏), Miss Jia Hui Bai (白佳惠) and Miss Jia Ling Zhan (詹佳玲) for the pleasant laboratory life and precious friendship.

Finally, I thank my family for concerned about me and unconditional support.

Index

Chapter 4
Experimental Results

Chapter 5
Conclusion and Future Work

Chapter 1
Introduction

1.1 History

X-ray was discovered at 1895 by Wihekm Conard Röntgen. Since X-ray has short wavelength and high penetrate power, it is often used in some applications about material studies and medical physics. X-ray has wavelength in the range of 100 to 0.1 angstrom (corresponding to energies in the range of 124eV to 124keV).

The first X-ray image was taken in 1895 by Rontgen, it was a picture of Anna Bertha Röntgen's hand. X-ray penetrated her hand, her ring and bones can be seen in this picture. The picture is shown below:

Fig. 1-1 Anna Bertha Röntgen's hand.

Röntgen found out that bony structures can be observed directly in X-ray image. As a result, X-ray began to be used in medical imaging.

In 1946, synchrotron radiation had been discovered in General Electric Research Laboratory. Synchrotron can generate collimated, coherent and linear polarized X-ray with continuous spectra, so the X-ray sources by synchrotron are energy-tunable with proper monochromator. There are many applications of synchrotron radiation light, such as X-ray crystallography(including X-ray diffraction, (XRD), X-ray reflectivity, small angle X-ray scattering (SAXS), Wide angle X-ray scattering

(WAXS) ,….ect.), X-ray fluorescence (XRF), X-ray absorption spectroscopy, and X-ray imaging.

X-ray microscopy is one of the applications of X-ray image. Since X-rays have short wavelengths, the spatial resolution can be improved with X-ray light source. The idea was proposed soon after the discovery of X-ray. But there were some problems, for examples, the X-ray sources were not intense enough, the lenses suit for X-ray and the high-resolution detectors were not available. X-ray microscopes became available until the synchrotron X-ray sources and useful focusing optical components were invented.

X-ray can't be focused by ordinary refractive lens, since the real part of refractive indies n of most of matters in the world are smaller than 1 in X-ray region (the interactions between X-ray and matter, and the dispersion relation will be explained in the following sections). In X-ray optical system, zone plates are often used to be X-ray lens. With e-beam lithography technologies, the fabrication of zone plate was improved. Therefore, X-ray image can be magnified, and the spatial resolution will be better. However, the spatial resolution is limited by the numerical aperture (NA) of zone plate. And qualities of the X-ray images depend on the quality of zone plate.

This thesis is mainly focused on the affections due to zone plate tilt in transmission X-ray microscope (TXM) system. So the principles of zone plates and TXM will be detailed introduced in next chapter.

1.2 **Light in Bulk Matter**

The refractive index is defined as:

$$n \equiv \frac{c}{v} = \sqrt{\frac{\varepsilon\mu}{\varepsilon_0\mu_0}} = \sqrt{\varepsilon_r\mu_r} \qquad (1.1)$$

, where v is the phase velocity of light in the medium, c is the speed of light in vacuum, ε is the permittivity, μ is the permeability, ε_0 and μ_0 are the permittivity and permeability of free space ($\varepsilon_r = \varepsilon / \varepsilon_0$ and $\mu_r = \mu / \mu_0$). In fact, the refractive index is frequency dependent. The dependence of n on wavelength/ frequency of light is the effect of dispersion.

When light waves impinge on a medium, they will interact with the atoms in the medium. Each atom can be thought as a classic forced oscillator being driven by the time-varying electric force $F_E = q_e E(t)$.

An electron which is displaced by a small distance x from equilibrium suffers the restoring force $m_e\omega_s{}^2 x$ and damping force $m_e\gamma\frac{dx}{dt}$, where ω_s is the resonance frequency, and x is the displacement between the negative cloud and the positive nucleus. If the directions of the restoring force and damping force of the electron are opposite to the direction of the driving force, by Newton's second law:

$$\begin{aligned} & F_E - m_e\omega_s{}^2 x - m_e\gamma\frac{dx}{dt} = m_e\frac{d^2x}{dt^2} \\ & \Rightarrow q_e\vec{E}(t) - m_e\omega_s{}^2 x - m_e\gamma\dot{x} = m_e\ddot{x} \end{aligned} \tag{1.2}$$

If the frequency of the electric field is ω, the light wave can be expressed as $E(t) = E_0\exp(j\omega t)$, and we can anticipate that the electron will oscillate at the same frequency. We assume the solution of displacement x is:

$$x(t) = x_0\exp(j\omega t)$$

$$\begin{aligned} & q_e E(t) - m_e\omega_s{}^2 x - m_e\gamma\dot{x} = q_e E(t) - m_e\omega_s{}^2 x - jm_e\gamma\omega x = -m_e\omega^2 x \\ & \Rightarrow q_e E(t) = q_e E_0\exp(j\omega t) = (\omega_s{}^2 + j\gamma\omega - \omega^2)m_e x \end{aligned}$$

$$\Rightarrow x(t) = \frac{q_e E_0\exp(j\omega t)}{m_e(\omega_s{}^2 - \omega^2 + j\gamma\omega)} \tag{1.3}$$

If the driving force FE is zero, the oscillator will vibrate at its resonance frequency ω_s.

1.3 The Dispersion Equation and Complex Refractive Index

The density of dipole moments P is:

$$P = \varepsilon_0\chi E = q_e xN \tag{1.4}$$

where N is the density of electrons (number of electrons per unit volume). By eq. (1.3), we can rewrite eq. (1.4) as:

$$P = \varepsilon_0\chi E = \frac{q_e{}^2 NE_0\exp(j\omega t)}{m_e(\omega_s{}^2 - \omega^2 + j\gamma\omega)}$$

$$\Rightarrow \varepsilon = \varepsilon_0(1+\chi) = \varepsilon_0 + \frac{P}{E} = \varepsilon_0 + \frac{{q_e}^2 N}{m_e({\omega_s}^2 - \omega^2 + j\gamma\omega)} \tag{1.5}$$

Setting the relative permeability μ_r to be 1, by eq. (1.1) the refractive index

$$n^2 = \frac{1}{\varepsilon_r} = \frac{\varepsilon}{\varepsilon_0}$$

$$\Rightarrow n^2(\omega) = \varepsilon_r = 1 + \frac{P}{E} = 1 + \frac{{q_e}^2 N}{m_e\varepsilon_0({\omega_s}^2 - \omega^2 + j\gamma\omega)} \tag{1.6}$$

Eq. (1.1) is known as the dispersion equation. We can see that, the refractive index is a function of the frequency.

If there are N molecules per unit volume, each with fj oscillators having resonant frequency, where j=1, 2, 3, …, and the dispersion equation can be expressed as:

$$n^2(\omega) = 1 + \frac{{q_e}^2 N}{m_e\varepsilon_0}\sum_i \frac{f_i}{({\omega_s}^2 - \omega^2 + j\gamma\omega)} \tag{1.7}$$

$$\Rightarrow n(\omega) = \sqrt{1 + \frac{{q_e}^2 N}{m_e\varepsilon_0}\sum_i \frac{f_i}{({\omega_s}^2 - \omega^2 + j\gamma\omega)}} \tag{1.8}$$

, where fi terms are weighting factors, and they satisfy the requirement:

$$\sum_i f_i = 1 \tag{1.9}$$

f_i terms are known as transition probabilities or oscillator strengths.

If ω^2 is much larger than $\frac{{q_e}^2 N}{m_e\varepsilon_0}$, eq. (1.8) can be approximated as:

$$n(\omega) = \sqrt{1 + \frac{{q_e}^2 N}{m_e\varepsilon_0}\sum_i \frac{f_i}{({\omega_s}^2 - \omega^2 + j\gamma\omega)}} \cong 1 + \frac{{q_e}^2 N}{2m_e\varepsilon_0}\sum_i \frac{f_i}{({\omega_s}^2 - \omega^2 + j\gamma\omega)}$$

$$\Rightarrow n(\omega) \cong 1 + \frac{{q_e}^2 N}{2m_e\varepsilon_0}\sum_i \frac{f_i}{({\omega_s}^2 - \omega^2)} - j\frac{{q_e}^2 N}{2m_e\varepsilon_0}\sum_i \frac{f_i}{\gamma\omega} = 1 - \delta + j\beta \tag{1.10}$$

, where $1-\delta$ and β are the real part and the imaginary part of the refractive index respectively. And

$$\delta = \frac{{q_e}^2 N}{2m_e\varepsilon_0}\sum_i \frac{f_i}{(\omega^2 - {\omega_s}^2)} \tag{1.11}$$

$$\beta = -\frac{{q_e}^2 N}{2m_e\varepsilon_0}\sum_i \frac{f_i}{\gamma\omega} \tag{1.12}$$

Since the frequencies of X-rays are large, the refractive indices are approximately unity. Besides, δ is usually positive, and the real part of refractive index is slightly less than1. By Snell's law, the refractive angle will be larger than the incident angle. Therefore, X-ray can't be focused by ordinary lenses, and conventional refractive optics is not suitable for X-ray.

The imaginary part of the refractive index, β, governs the absorption. Consider a light wave $E(r,t) = E_0 \exp[j(\omega t - kr)]$ propagates in a medium with refractive $n = 1 - \delta + j\beta$, where k is the wave vector,

$$k = \frac{2n\pi}{\lambda} = \frac{2\pi}{\lambda}(1 - \delta + j\beta) = k_0(1 - \delta + j\beta) \tag{1.13}$$

, where $k_0 = \frac{2\pi}{\lambda}$. As a result, the optical field will become:

$$E(r,t) = E_0 e^{j(\omega t - k_0 r)} e^{jk\delta r} e^{-k\beta r} \tag{1.14}$$

The first term is the original wave in vacuum, the second term is due to the phase retardation, and the third term is the attenuation. The intensity of the wave is:

$$I(r,t) = E(r,t)\cdot E^*(r,t) = {E_0}^2 e^{-2k\beta r} \tag{1.15}$$

The amount of phase retardation is:

$$\phi = k_0 \delta r \tag{1.16}$$

, and the absorbed energy is:

$$E_0{}^2 (1 - e^{-2k\beta r}) \tag{1.17}$$

Chapter 2
Transmission X-ray Microscope (TXM) at NSRRC

Transmission X-ray microscope (TXM) is one of the X-ray microscopes. NSRRC's TXM was designed and installed in September 2004 by NSRRC and Xradia, it was the first zone plate based hard X-ray microscope operated at 8-11 keV. The resolution of this TXM is about 60 nm in hard X-ray region.

My experiment is performed in this end station. The structure, optical components and principles of the TXM system will be introduced in this chapter.

2.1 The Structure of TXM

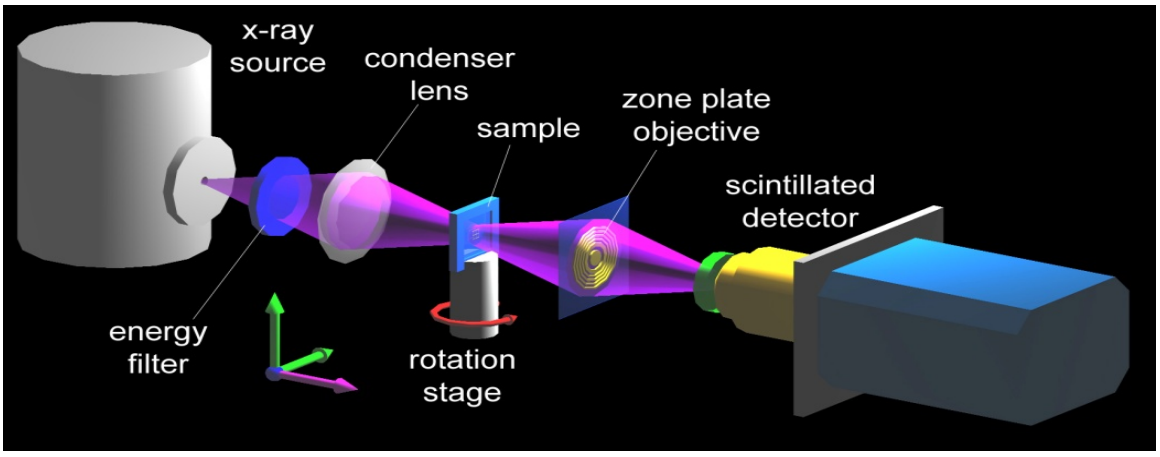

Fig. 2-1 The structure of TXM system. The zone plate can be regarded as a X-ray lens.

The structure of TXM system is shown in Fig. 2-1. X-ray come out from the synchrotron, pass through the energy filter and the condenser. Photons with energy from 8 to 11 keV are filtered through the energy filter. After passing through the condenser, X-rays become convergent, hollow cone, and focused on the sample. The zone plate which is put behind the sample acts as an objective lens in microscope. In the scintillated system, the scintillator converts X-ray to visible light, and the CCD gets the image. By Fourier theory, the optical wave distribution can be calculated, if we know the original wave function, the distances between each element, and the transparencies of the sample and zone plate. Those elements in TXM system will be introduced in the following sections.

2.1.1 The Light Source of TXM System

The Taiwan Light Source (TLS) is a 1.5GeV synchrotron, constructed in October 1993 in Hsin Chu, Taiwan, also and it was the first third generation synchrotron in Asia. The NSRRC's TXM is in beam line BL01B end station.

Synchrotron is a kind of cyclic particle accelerator. The electric and the magnetic fields are carefully synchronized with the traveling particle beam in the synchrotron. The electric force accelerates the particles. The particles circulate, because the magnetic force $\vec{B}$ is perpendicular to the direction of velocity $\vec{v}$ of the particles. In order to enhance the intensity of X-ray, the insertion devices (IDs) are inserted into a straight section of the storage ring. Insertion devices are composed of arrays of magnets, and they generate spatial periodic magnetic field. When charged particles pass through an insertion device, the magnetic fields will generate transverse acceleration of the particles, which emit the synchrotron radiation in the projection direction. With the help of IDs, the synchrotron radiation is highly-brilliant, forward-directed and quasi-monochromatic. In beam line BL01B at NSRRC, an insertion device, superconducting wavelength shifter (SWLS) was installed at the downstream of the straight section.

The beam line BL01B is about 30 meters long from the front to the end station, it was composed of two optical components, the focusing mirror(FM), and the double crystal monochromator (DCM). The FM is used to focus X-ray to the sample, and the DCM which consists of two Ge(111) crystals can give the resolving power up to 1000. The photon beams filtered through the DCM are monochromatic with energies tunable from 5keV to 20keV with an expect photon flux about $7\times10^{11}\ photons/\sec/200mA$ (an photon flux of $5\times10^{11}\ photons/\sec/300mA$ has been measured) with an average energy resolution ($\Delta E/E$) of 1×10^{-3}. The beam spot is about $1mm\times0.3mm$ at the end of the beam line, the emittance in horizontal and vertical directions are different.

A shutter and an ion chamber are placed between the X-ray source and the TXM system. Shutter can protect the optical system from…, and the ion chamber is used to measure the X-ray flux.

2.1.2 Condenser

The condenser in TXM system is a 15 cm-long, circularly symmetric single

reflection glass capillary. The reflection angle is about 0.5mrad respect to the propagation direction, and the measured reflection angle from the condenser is from 0.87 mrad. to 1.13mrad. The total internal reflection gives the reflection up to 90% for 8keV at 0.5 mrad. The limitation of the critical angle for the condenser is about 4 mrad. for the roughness is about 10nm. The shape of the capillary is hyperbolic type and made by the capillary puller in Xradia Inc. Fig. 2-2 shows the structure of the condenser.

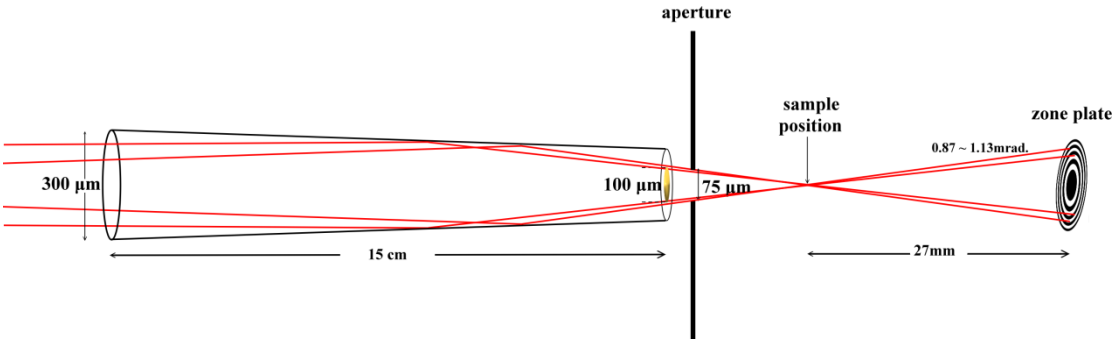

Fig. 2-2 The optical layout of the condenser.

The diameters of entrance and exit are about 300 µm and 200 µm, respectively. Since the foot print of the X-ray beam is about $1mm \times 0.3mm$ (horizontal × vertical) on the entrance of the condenser, the condenser will make flux loss in the horizontal. As shown in Fig. 2-2, there is a gold bead of 100 µm which blocks X-ray at the end of the condenser, so the output of the condenser is the hollow cone beam. The beam comes out from the condenser will focus at the sample position. There is a low resolution CCD camera which can be placed in the beam path in the microscope to monitor the shape and flux of the focal spot.

2.1.3 Zone Plate

In TXM system, the zone plate is made of gold on the silicon nitride membrane by electron beam lithography, it acts as a focal lens. The distance between the zone plate and the sample is equal to the focal length of zone plate, 27mm. And the zone plate of 75 to 85 μm diameter is illuminated by the hollow cone beam from the condenser. A zone plate consists of many concentric rings. Light passing through the zone plate will diffract around the rings. And the zone plate uses diffraction to focus light. The principle of zone plate will be explained later.

The zone plate has a diffraction-limited resolution:

$$\delta_m = K_1\lambda/NA = 2K_1 dr/m \quad (2.1)$$

, where m is the diffraction order, and dr is the width of the outmost ring, $0.3 \le K_1 \le 0.61$, depending on the illumination condition. In TXM system, $K_1 = 0.61$, the resolution is given by δ_m=1.22dr/m.

The outmost ring width of the zone plate is 50mn in TXM system, so the spatial resolution of first order is about 60nm. By the way, the aspect ratio of zone plate is defined as:

$$\text{Aspect ratio} \equiv \frac{h}{dr} \quad (2.2)$$

where h is the thickness of zone plate.

The optimal thickness of zone plate is about 1.8 μm to achieve a phase shift of π at 8 keV (the aspect ratio is about 36). Since the achievable aspect ratio for gold zone plate was about 18 when TXM is installed, the fabrication of an ideal zone plate which can achieve a phase shift of π is still a big challenge. In order to achieve phase shift of π/2 at 8keV, the thickness of gold has to be about 890nm, the calculation is shown below:

By eq. (1.10), the complex refraction index can be expressed as n=1-δ+iβ. For gold, $\delta \approx 4.2*10^{-5}$ at 8 keV (Ref [2])

$$\text{Phase shift } \Delta\varphi = \frac{2\delta\pi}{\lambda} \times h = \frac{2 \times 4.2 \times 10^{-5} \times \pi}{1.5 \times 10^{-10}} \times h = \frac{\pi}{2} \Rightarrow h = 890 \times 10^{-9}$$

The aspect ratio is about 18. To fabricate a zone plate of high aspect ratio is difficult.

2.1.4 Scintillated System

The scintillated system in TXM is composed of the scintillator and the CCD detector, the scintillated system is shown in Fig. 2-3.

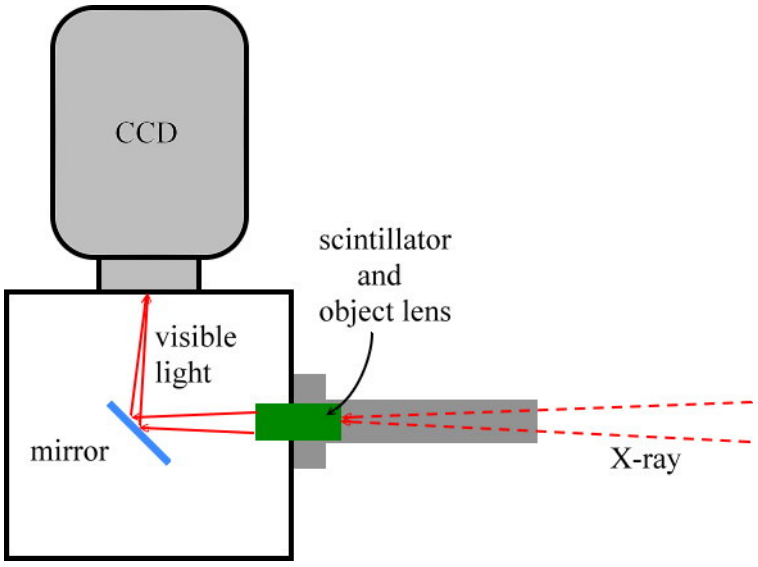

Fig. 2-3 The internal structure of scintillated system.

The scintillator is able to convert X-ray to the visible light. The scintillator is made of CsI with the quantum efficiency up to 40% at 8keV. There is a visible-light 20× objective lens behind the scintillator, the object lens is used to magnify the image on the scintillator. And the magnified image will be reflected to a CCD by a mirror with 45 degree. The CCD is PIXIS 1024, which has 1024×1024 pixels with readout rate of 20Mbit/sec.

There is a flight tube filled with helium between the zone plate and the scintillated system. Since the flux of X-ray decays fast in the air, the helium is purged into the flight tube to suppress the flux decay. If the whole system can be installed in vacuum, the flux of X-ray will be maintained very well.

2.2 Wave Propagation

By Fourier optics theory, optical waves are described as a weight sum of plane waves with different spatial frequencies. We can calculate the propagation of optical waves through various optical systems. Fourier optics uses the spatial frequency domain as the conjugate of the spatial domain, and Fourier transform (FT) theory is often used as a tool to solve the problems of wave propagation.

In general, a homogeneous optical wave can be expressed as a weighted superposition of elementary plane wave solutions:

$$U(x,y)=\int_{-\infty}^{\infty}\int_{-\infty}^{\infty}U(f_x,f_y)\cdot e^{j2\pi(f_x x+f_y y)}df_x df_y \qquad (2.3)$$

, where f_x and f_y are the spatial frequency, and $U(f_x, f_y)$ represents a plane wave with spatial frequency of (f_x, f_y). The plane wave spectrum representation of the optical field is the basic foundation of Fourier optics. We can see that, the above equation is an inverse Fourier transform of the plane wave $U(f_x, f_y)$.

$$\begin{aligned} &U(x,y) = F^{-1}\{U(f_x, f_y)\} \\ &\Rightarrow U(f_x, f_y) = F\{U(x,y)\} \end{aligned} \tag{2.4}$$

Consider two points P_1 and P_0 on the (X,Y) plane and the (x,y) plane respectively, as shown in Fig. 2-4. The Heygens-Fresnel principle can be stated as:

$$U(P_0) = \frac{1}{j\lambda}\int_{-\infty}^{\infty}\int_{-\infty}^{\infty} U(P_1)\cdot\frac{\exp(jkr_{01})}{r_{01}}\cdot\cos\theta\cdot ds \tag{2.5}$$

, where k is the wave vector, λ is the wavelength, $r_{01} = \overline{P_0P_1}$, and θ is the angle between $\vec{r}_{01}$ and the optical axis.

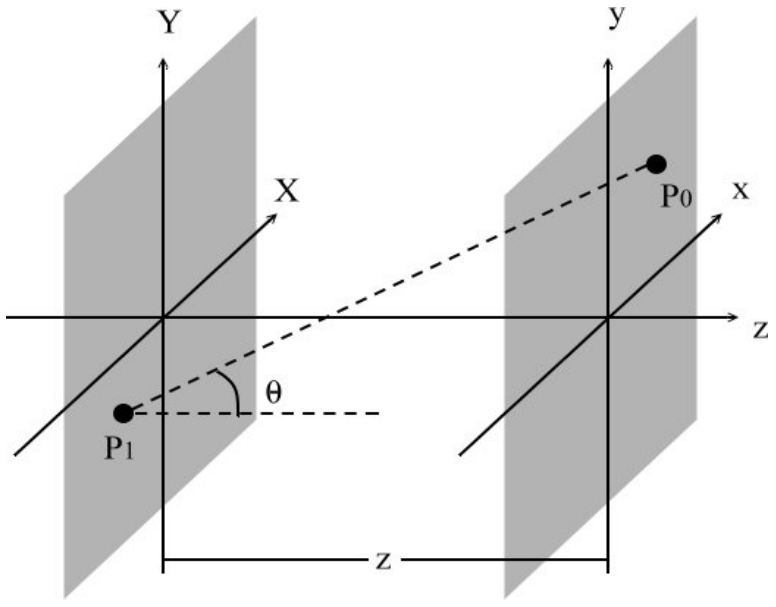

Fig. 2-4 Diffraction Geometry

The optical field at P_0=(x,y) is expressed as:

$$U(x,y)=\frac{1}{j\lambda}\int_{-\infty}^{\infty}\int_{-\infty}^{\infty}U(X,Y)\cdot\frac{\exp[jk\sqrt{(x-X)^2+(y-Y)^2+z^2}]}{\sqrt{(x-X)^2+(y-Y)^2+z^2}}\cdot\cos\theta\cdot dXdY \qquad (2.6)$$

, where $\cos\theta=\frac{z}{\sqrt{(x-X)^2+(y-Y)^2+z^2}}$. If $z^2>>(x-X)^2+(y-Y)^2$, then

$$\sqrt{(x-X)^2+(y-Y)^2+z^2}\cong z[1+\frac{(x-X)^2+(y-Y)^2}{2z^2}]=z+\frac{(x-X)^2+(y-Y)^2}{2z}$$

$$U(x,y)$$
$$=\frac{1}{j\lambda}\int_{-\infty}^{\infty}\int_{-\infty}^{\infty}U(X,Y)\cdot\frac{\exp[jk\sqrt{(x-X)^2+(y-Y)^2+z^2}]\cdot z}{(x-X)^2+(y-Y)^2+z^2}\cdot dXdY$$

$$\cong\frac{1}{j\lambda}\int_{-\infty}^{\infty}\int_{-\infty}^{\infty}U(X,Y)\cdot\frac{\exp(jkz)\cdot\exp\{k\cdot[(x-X)^2+(y-Y)^2)]/2z\}}{z}\cdot dXdY$$
$$=\frac{\exp(jkz)}{j\lambda z}\int_{-\infty}^{\infty}\int_{-\infty}^{\infty}U(X,Y)\cdot\exp\{k\cdot[(x-X)^2+(y-Y)^2)]/2z\}\cdot dXdY$$
$$=\int_{-\infty}^{\infty}\int_{-\infty}^{\infty}U(X,Y)\cdot p(x-X,y-Y))]\cdot dXdY$$
$$=U(X,Y)\otimes p(X,Y) \qquad (2.7)$$

The above equation is seen to be a convolution, where

$$\text{p(x,y)}=\frac{\exp(jkz)}{j\lambda z}\cdot\exp[k\cdot(x^2+y^2)/2z] \qquad (2.8)$$

is the propagator in real space. Another form of the result can be written as:

$$U(x,y)$$
$$\cong\frac{\exp(j2k)}{j\lambda z}\int_{-\infty}^{\infty}\int_{-\infty}^{\infty}U(X,Y)\cdot\exp\{k\cdot[(x-X)^2+(y-Y)^2)]/2z\}\cdot dXdY$$
$$=\frac{\exp(jkz)}{j\lambda z}\cdot\exp[j\frac{k}{2z}(x^2+y^2)]\cdot\int_{-\infty}^{\infty}\int_{-\infty}^{\infty}U(X,Y)\cdot\exp[j\frac{k}{2z}(X^2+Y^2)]\cdot\exp[j\frac{2\pi}{\lambda z}(xX+yY)]dXdY$$
$$=\frac{\exp(jkz)}{j\lambda z}\cdot\exp[j\frac{k}{2z}(x^2+y^2)]\cdot F\{U(X,Y)\cdot\exp[j\frac{k}{2z}(X^2+Y^2)]\} \qquad (2.9)$$

We refer to the forms of the result of eq. (2.7) and (2.9), as the Fresnel diffraction integral. By convolution theorem,

$$U(X,Y)\otimes p(X,Y)=F^{-1}\{U(f_x,f_y)\cdot P(f_x,f_y)\} \qquad (2.10)$$

, where $U(f_x,f_y)=F\{u(x,y)\}$ and $P(f_x,f_y)=F\{p(x,y)\}$.

By the results of eq. (2.7) and (2.10), we can calculate the wave function of the propagated wave, as long as we know the original wave function and the propagation distance.

2.3 Principle of Zone Plate

In section 2.1, the zone plate and other optical components in TXM system have been introduced. Zone plates were created by Augustin-Jean Fresnel, so they are also known as Fresnel zone plates. A zone plate consists of many concentric ring-shaped zones, known as Fresnel zones. Alternate zones are open the others block the incident beam (amplitude zone plate), or advance/retard the phase of incident beam (phase zone plate).

2.3.1 Amplitude Zone Plate

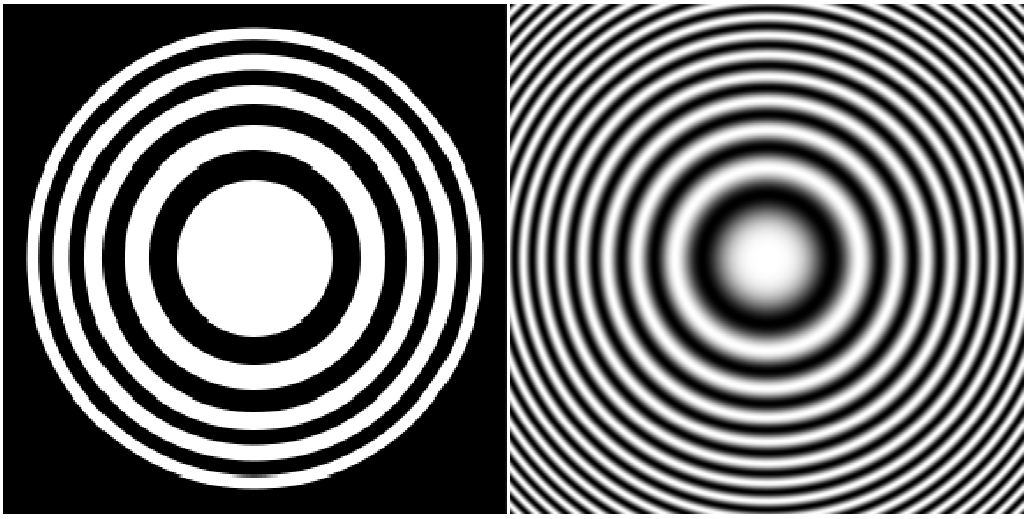

(a) (b)

Fig. 2-5 (a) Binary zone plate, it focuses light at many points. (b) Sinusoidal zone plate, it has one focal point.

There are two types of amplitude zone plates in Fig. 2-5, the binary zone plate and the sinusoidal zone plate. The transmittance of a binary zone plate must be 1 or 0. That is, the rings of binary zone plate are completely opaque. But the transmittance of a sinusoidal zone plate varies gradually in a sinusoidal manner. Besides, a binary zone plate has many focal points, but a sinusoidal zone plate has only one focal point.

Light passing through zone plate will diffract around the rings. Unlike optical or reflective type lenses, zone plates use diffraction of X-ray to focus light rather than

using refraction. If the optical waves are all in phase, the focal spot will total constructively interfere. As a result, we can see a focus spot behind the zone plate.

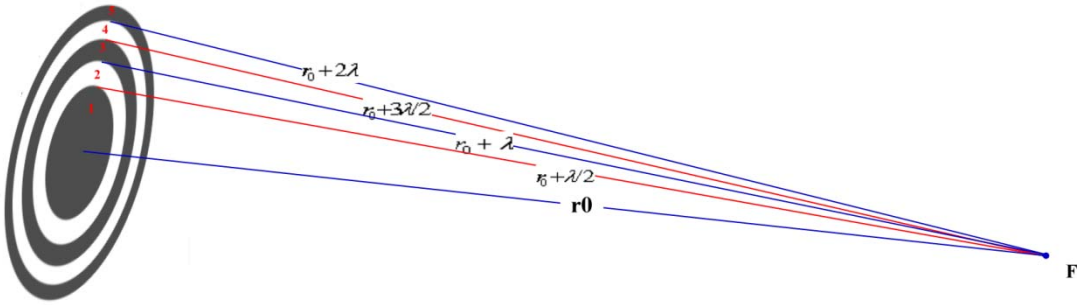

Fig. 2-6 A zone plate obstructs the blue paths. Only the optical waves come from red paths can pass through the zone plate. The phase differences of the waves are equal to multiples of 2π at focal point.

The radiuses of the Fresnel zones are related to the focal length of zone plate and the wavelength of incident beam. In Fig. 2-6, the blue lines and red lines are optical paths. The optical path length difference (OPD) between any two paths of the same color is a multiple of the wavelength, so the phase difference is a multiple of 2 π . That is, the optical waves from the paths of the same color are all in phase. However, the optical waves from the paths of different colors are out of phase (the OPD is $\lambda / 2$). As shown in Fig. 3-1, the zone plate obstructs the blue paths, the optical waves come from red paths will constructively interfere at the focal point. If we remove the red lines, let blue lines pass, it won't change the wave distribution on the image plane. Zone plates produce equivalent diffraction patterns no matter whether the central disk is opaque or transparent.

Since the OPD between two nearby zones is $\lambda / 2$, the radius of the zones are required to be (Ref [3]):

$$r_n = \sqrt{nf\lambda + \frac{n^2\lambda^2}{4}} \qquad (2.11)$$

, where r_n is the radius of the nth zone. If $f >> n\lambda$, eq. (2.11) can be simply expressed as:

$$r_n = \sqrt{nf\lambda + \frac{n^2\lambda^2}{4}} \cong \sqrt{nf\lambda} \tag{2.12}$$

In this approximation, all zones have the same areas and contribute equally to the irradiance at the focal point.

2.3.2 Phase Zone Plate

Unlike the amplitude zone plates, the phase zone plates change the phase of incident beam. This is done by adding or subtracting the optical path length in the zones, using refractive material of appropriate thickness. The transmission function of a pure phase zone plate can be expressed as (Ref [1]):

$$T(x,y) = \exp\{-i\pi[\frac{1}{2} + \frac{2}{\pi}\sum_{m=1,3,5...}^{\infty} C_m \sin(m\pi\frac{x^2+y^2}{\lambda f})]\} \tag{2.13}$$

, where m is the diffraction order, f is the focal length of zone plate, λ is the wavelength, and C_m=1/m is the weight of each diffraction number. The term 1/2 represents the non-diffraction zero order background, and m=1, 3, 5,… represent for the first, the third, the fifth order, etc. The absolute value of T is 1, the phase zone plate doesn't change the intensity of incident beam, it only changes the phase term. By the transmission function, we can see that, the cross-section of zone plate is approximately rectangular shape.

There are many diffraction orders behind a phase zone plate, and they focus at different focal points, as shown in Fig. 2-7. The focal length is inverse proportional to the diffraction order, focal length of m th order is f_m=f/m. As a result, the phase zone plate can be regarded as a lens with many focal points.

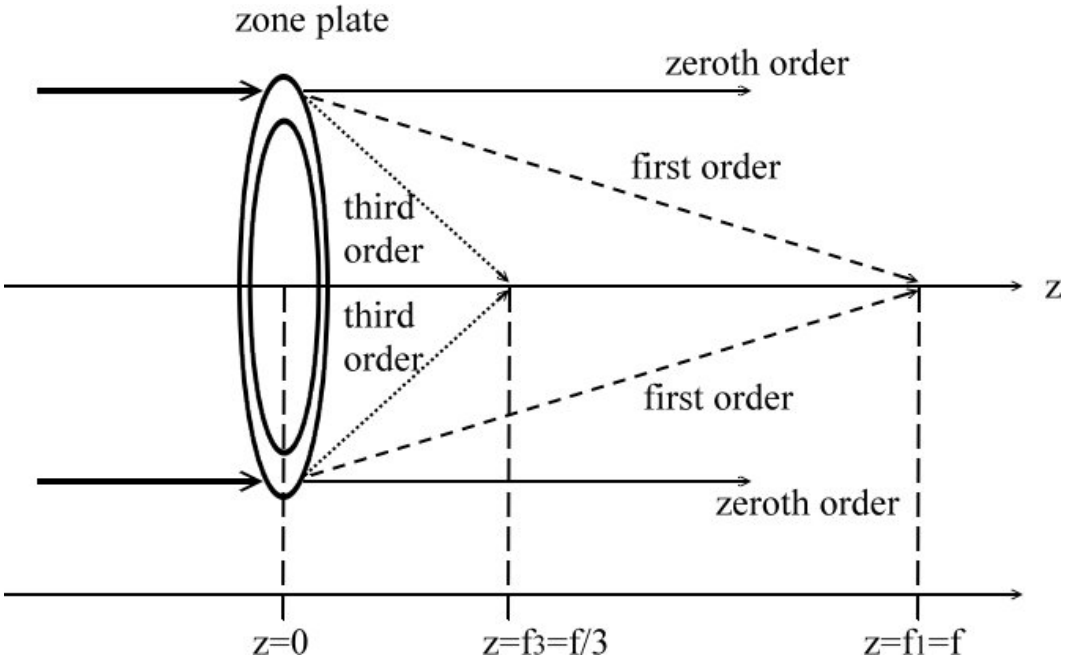

Fig. 2-7 Light waves diffract around zone plate, and there will be many diffraction orders behind the zone plate (It only shows the zero order, first order, and the third order in this picture). The focal length of each order is inversed proportional to the diffraction order.

As a result, the zone plate can be regarded as a lens with many focal points. Besides, the focal length f, numerical aperture (NA), and the diffraction-limit resolution δ of zone plate are related to the radius and the width of the outmost ring, r and dr, the diffraction order m, and the wavelength λ. The following equations show the relationships (Ref[1]):

$$f_m=f/m=\frac{2rdr}{m\lambda} \tag{2.14}$$

$$NA=\frac{m\lambda}{2dr} \tag{2.15}$$

$$\delta_m=\frac{K_1\lambda}{NA}=\frac{2K_1dr}{m} \tag{2.16}$$

, where $0.3 \le K_1 \le 0.61$, depending on the illumination condition. In TXM system, the resolution is given by δ_m=1.22dr/m.

By the equations, we can see that the higher the diffraction order, the shorter the focal length, the larger the numerical aperture, and the better the resolution.

Chapter 3

The Simulation of Wave Propagation and Affections Due to Zone Plate Tip / Tilt in TXM

The structure of TXM and the optical components in TXM system is introduced in chapter 2. There are some simulation results in this chapter. A Matlab program is designed to calculate the optical fields in TXM system, and it also can calculate the transmission function of a tipped / tilted zone plate. There are some simulated images acquired at different tip / tilt angles, the images will be compared and the relationship between the image quality and the tip / tilt angle will be discussed.

In this chapter, the calculation of X-ray optical fields in TXM system is based on the paraxial approximation in scalar wave field theory (Ref. [4]). The approximation requires that the propagation distances are much larger than the wavelength and that the sample and zone plate can be described by thin element transmission functions. Besides, quasi-monochromatic object illumination conditions are assumed. We set the wave length of X-ray to be 1.5 angstrom (the photon energy is about 8.27keV) in our calculation and simulation.

3.1 Wave Propagation in TXM System

3.1.1 Calculations of Optical Fields

The optical fields in TXM system can be calculated by Fourier optics theory which has been introduced in section 2.2.

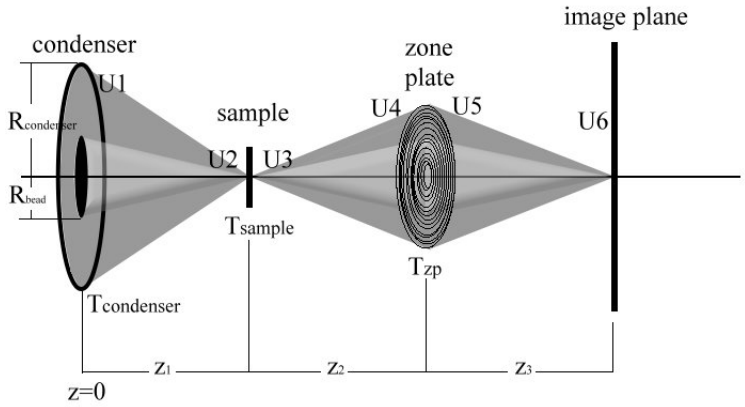

Fig. 3-1 Optical wave propagates from the condenser to the image plane. The

distances between each element are z_1, z_2, z_3, and $\frac{1}{z_2}+\frac{1}{z_3}=\frac{1}{f}$, f is the focal length of the zone plate. U_1, U_2, U_3, U_4, U_5, U_6 are the optical fields at z=0, $z=z_1^-$, $z=z_1^+$, $z=(z_1+z_2)^-$, $z=(z_1+z_2)^+$, $z=z_1+z_2+z_3$,respectively. $T_{condenser}$, T_{sample}, T_{ZP} are the transparencies of the condenser, the sample and the zone plate.

A part of the TXM system (from the condenser to the image plane of the zone plate), and the optical fields at many positions are shown in Fig. 3-1. U_1 is the optical field at the output of the condenser, it's convergent, hollow cone beam. The wave function U_1 can be calculated by multiplying a spherical wave U_0 by the transparency $T_{condenser}$. That is,

$$U_1(x,y)=U_0(x,y)\cdot T_{condenser}(x,y) \tag{3.1}$$

, where

$$U_0(x,y)=A\cdot\exp(jk\frac{x^2+y^2}{2z_1})=U_0(r)=A\cdot\exp(jk\frac{r^2}{2z_1}) \tag{3.2}$$

, and

$$T_{condenser}(x,y)=\begin{cases}1, R_{bead}<r=\sqrt{x^2+y^2}<R_{condenser}\\ 0, otherwise\end{cases} \tag{3.3}$$

By eq. (2.10),

$$U_2(x,y)=U_1(x,y)\otimes p_{z1}(x,y)=F^{-1}\{U_1(f_x,f_y)\cdot P_{z1}(f_x,f_y)\} \tag{3.4}$$

, where

$$p(x,y,z)=\frac{\exp(jkz)}{j\lambda z}\cdot\exp[k\cdot(x^2+y^2)/2z] \tag{3.5}$$

, and $p_{z1}(x,y)=p(x,y,z_1)$.

We can calculate the optical field U_3 by multiple U_2 and the transparency of the sample T_{sample}.

$$U_3(x,y)=U_2(x,y)\cdot T_{sample}(x,y) \tag{3.6}$$

$$U_4(x,y) = U_3(x,y) \otimes p_{z2}(x,y) = F^{-1}\{U_3(f_x, f_y) \cdot P_{z2}(f_x, f_y)\} \tag{3.7}$$

, where

$$p_{z2}(x,y) = p(x,y,z_2) = \frac{\exp(jkz_2)}{j\lambda z_2} \cdot \exp[k \cdot (x^2 + y^2)/2z_2] \tag{3.8}$$

$$U_5(x,y) = U_4(x,y) \cdot T_{ZP}(x,y) \tag{3.9}$$

, the transmission function of the zone plate T_{ZP} is shown in eq. (2.3) .

$$U_6(x,y) = U_5(x,y) \otimes p_{z3}(x,y) = F^{-1}\{U_5(f_x, f_y) \cdot P_{z3}(f_x, f_y)\} \tag{3.10}$$

, where

$$p_{z3}(x,y) = p(x,y,z_3) = \frac{\exp(jkz_3)}{j\lambda z_3} \cdot \exp[k \cdot (x^2 + y^2)/2z_3] \tag{3.11}$$

3.1.2 Wave Distributions

By eq. (3.1-11), if the distances z1, z2, z3, the optical field U_1, and the transparencies of sample and zone plate are know, the optical field at each position in Fig. 3-1 can be calculated. The calculations were implemented by using a Matlab code, and there is an example in this section. In this example, the wavelength of X-ray is 1.5 Å (the energy of a photon is about 8keV), the focal length of zone plate f=27mm, z_1=f=27mm, $z_2=\frac{10}{9}f$, z_3=10f, $R_{condenser} = 30.5\mu m$, $R_{bead} = 27.5\mu m$.

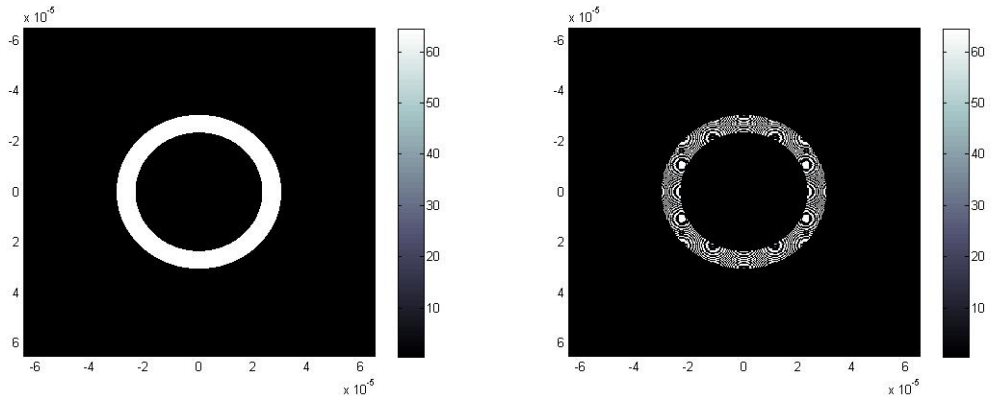

(a) (b)

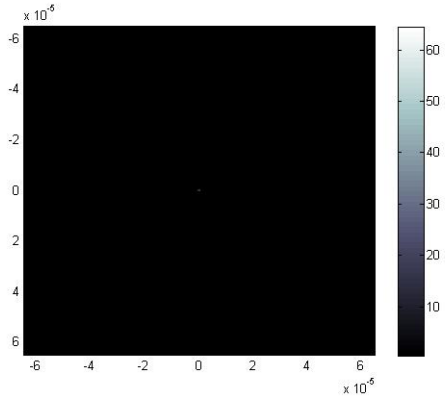

(c)

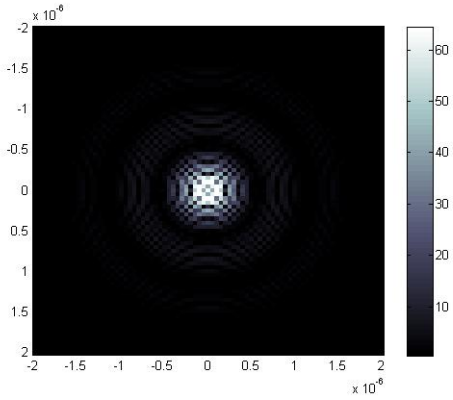

(d)

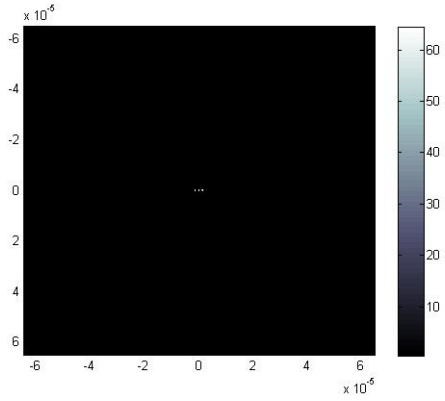

(e)

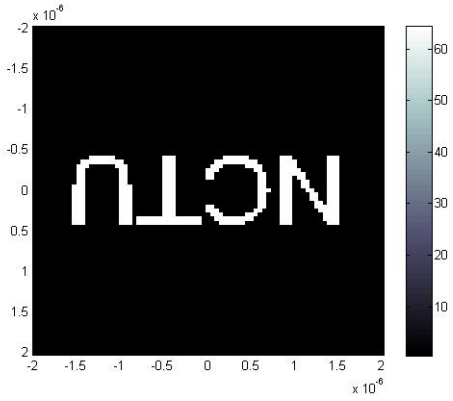

(f)

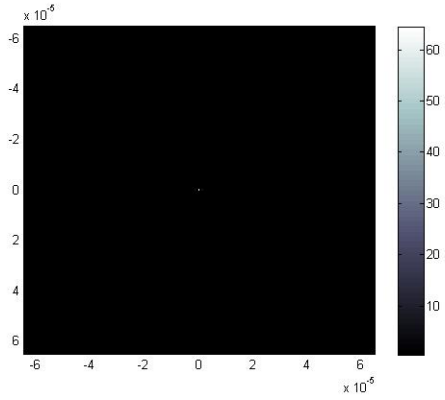

(g)

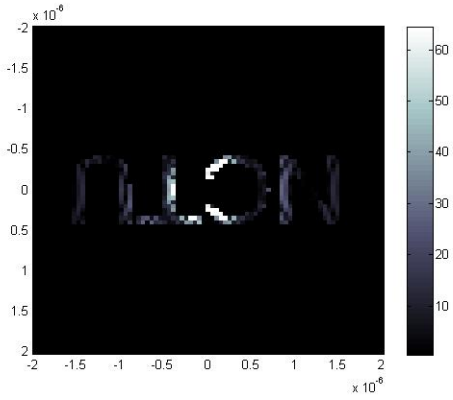

(h)

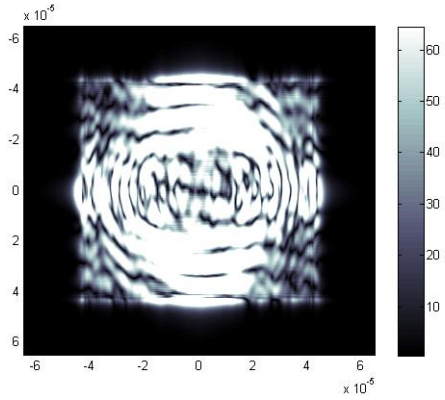

(i)

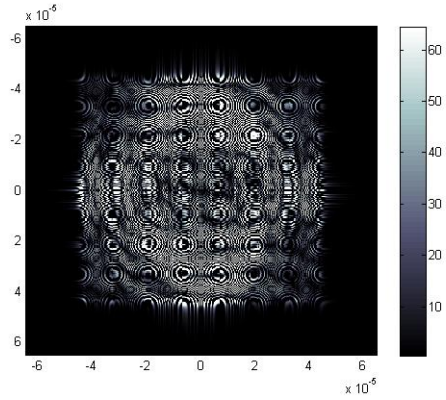

(j)

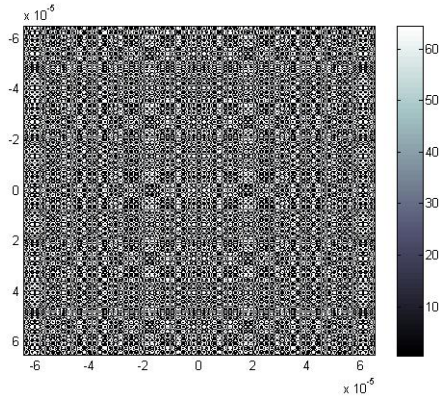

(k)

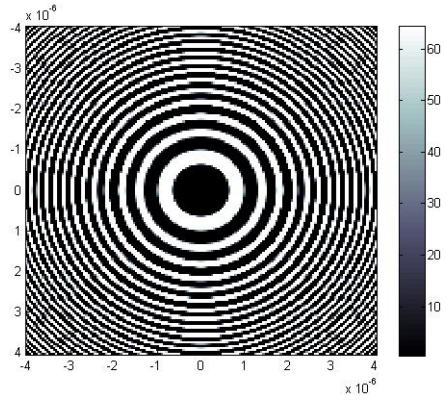

(l)

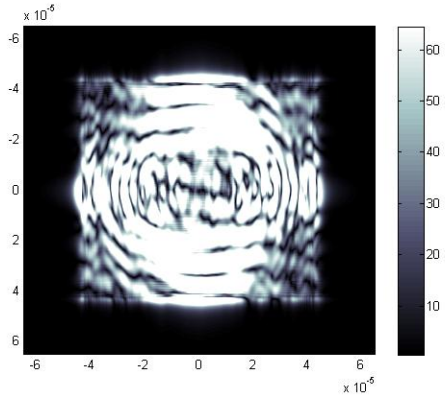

(m)

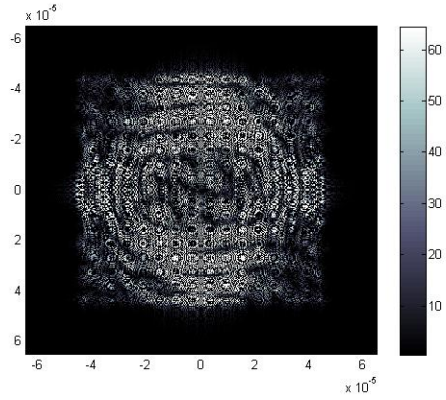

(n)

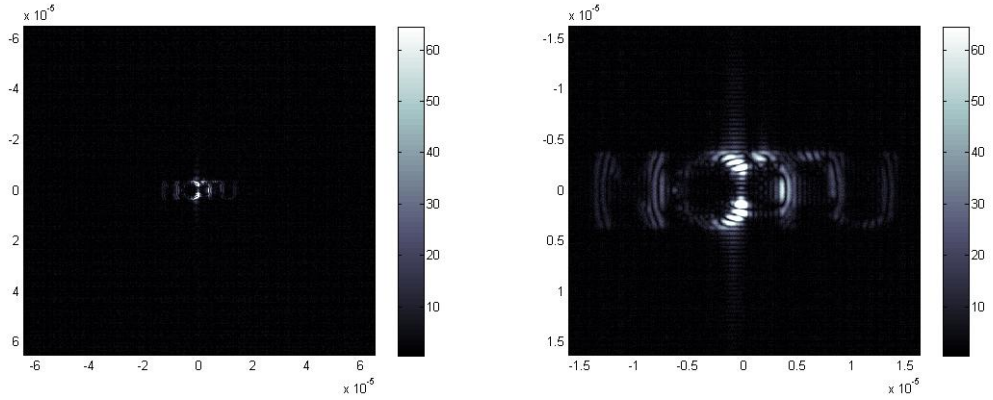

(o) (p)

Fig. 3-2 (a) The amplitude of U_1, $|U_1|$. (b) The phase of U_1. (c) The amplitude of U_2, $|U_2|$. (d) The magnified version of (c). (e) The transparency of the sample, T_{sample}. (f) The magnified version of (f). (g) The amplitude of U_3, $|U_3|$ (h) The magnified version. (i) The amplitude of U_4, $|U_4|$. (j) The phase of U_4. (k) The imaginary part of the transparency of a phase zone plate, $Im\{T_{ZP}\}$. The focal length of this zone plate is 27 mm at 8keV. (l) The magnified version of (k). (m) The amplitude of U_5, $|U_5|$. (n) The phase of U_5. (o) The amplitude of U_6, $|U_6|$. (p) The magnified version of (o).

The transparency of the sample, T_{sample}, is shown in Fig. 3-2 (e) and (f), it is reversal "NCTU". Fig. 3-2 (k), (l) show the imaginary part of the phase zone plate with 27mm focal length at 8 keV, we can see that the zone plate is composed of many concentric rings.

Since the optical field U_1 at z=0 is a convergent spherical wave with curvature $R=z_1$, after it propagates for a distance z_1, the beam will be focused to be a small spot on the sample; and the optical field at $z= z_1$ is U_2, as shown is Fig. 3-2 (c) and (d). The sample filters some X-rays out, so the shape of U_3 is like the sample. After the beam propagates for z_2, the wave distribution of U_4 is blurred, as shown is Fig. 3-2 (i). The amplitude distributions of U_4 and U_5 are the same, because the phase zone plate doesn't change the amplitude of the incident beam. However, the phases of U_4 and U_5 are different, as shown in Fig. 3-2 (j) and (n). The phase zone plate focuses the beam on the image plane, and the wave amplitude distribution on the image plane is shown in Fig. 3-2 (o) and (p). Compare Fig. (h) and (o), we can find out that the image is a reversed, magnified replica of the sample, and the magnification is $\frac{z_2}{z_3} = 9$. There are diffraction-like features in Fig. 3-2 (d) and (p) since the light source is coherent.

In Fig. 3-2 (h), we can see that, the X-ray can't illuminate the whole pattern of the sample, since the spot size of X-ray on the sample is too small. In fact, the output of the condenser is not ideal spherical wave, so the X-ray won't be focus to be a small spot on the sample. The problem can be solved by using a radial symmetric optical wave which can be expressed as

$$U_0(x,y) = A \cdot \exp(jk_r\sqrt{x^2+y^2}) = U_0(r) = A \cdot \exp(jk_r r) \tag{3.12}$$

to be U_0 instead of using the ideal spherical wave U_1 in Eq. (3.2), where $k_r = k\cos(0.87\text{mrad})$. In this way, the spot size of X-ray on the sample will be larger, the pattern of the sample can be completely illuminated, and the simulated TXM image will be better, as shown in Fig. 3-3.

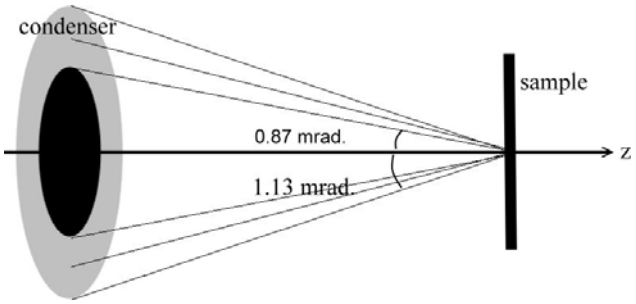

(a)

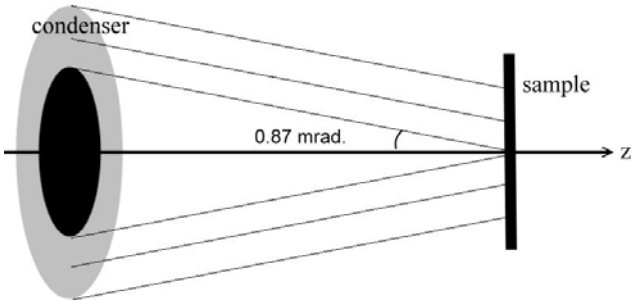

(b)

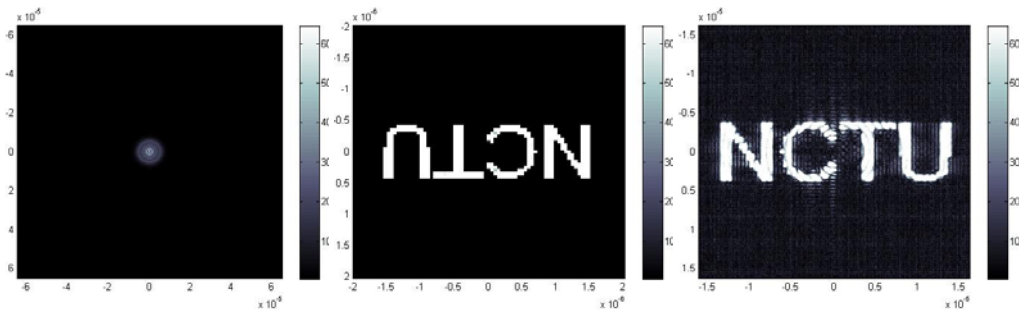

(c) (d) (e)

Fig. 3-3 (a) The output of the condenser is an ideal spherical wave. The X-ray will be focused to be a small spot on the sample. (b) The output of the condenser is not a ideal spherical wave. (c) The amplitude of U2, $|U_2|$. The spot size of X-ray on the sample is much larger in this picture than in Fig. 3-2 (c). (d) The amplitude of U_3, $|U_3|$. (e) The amplitude of U_6, $|U_6|$, magnified version.

3.2 Zone Plate Tilt and Affections

3.2.1 Aberration of Lens

According to geometrical optics theory, we can expect that the image will be affected by aberration when the lens is tilted (or the incident beam is oblique).

When the lens is tilted, i.e., the object point is away from the optical axis, the cone of incident beam will strike the lens asymmetrically, giving rise to a third primary aberration known as astigmatism. As a result, the focal lengths of horizontal rays and vertical rays are different, as shown in Fig. 3-4.

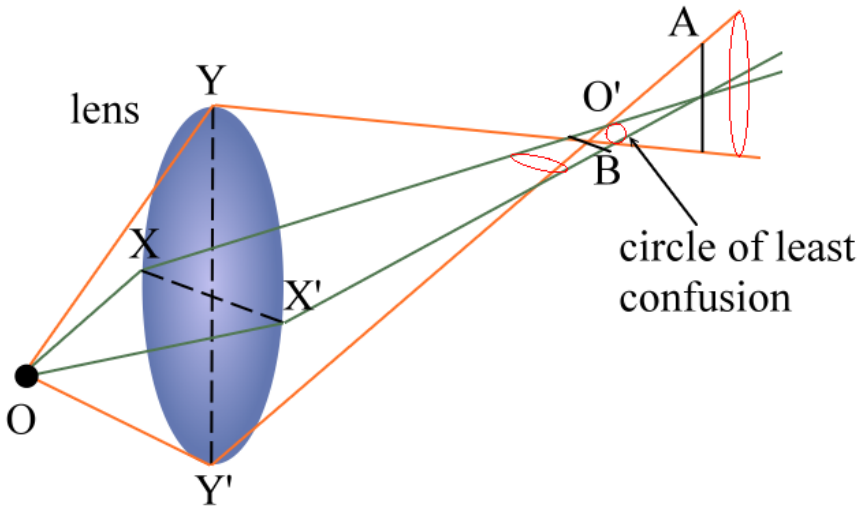

Fig. 3-4 Astigmatism of a lens.

The cross section of the beam as it leaves the lens is initially circular, but it becomes elliptical gradually, and then the ellipse degenerates into a line at the focal point of vertical rays, B. The line is known as the primary image. Beyond the focal point B, the cross section of the beam opens out, and it becomes circular again at O'. At O', the image is a circular blur known as the circle of least confusion. At the focal point of horizontal rays, A, the cross section of the beam becomes a line again, the line is known as the secondary image. The primary and secondary images are

perpendicular to each other. Beyond A, the cross section becomes elliptical. In addition, the size of the circle of least confusion increases as the focal length difference increases.

3.2.2 Zone Plate Tilt

The shape of zone plate's transmission function will look different for incident beam when zone plate is tilted. The relationship between the tilt angle and the effective transmission function of the zone plate will be discussed. In this section, T represents the original transmission function of a zone plate, T' represents the effective transmission function of the tilted zone plate, and θ is the tilt angle.

Assume that the rings of zone plate are opaque, that is, the relationship between the transparency and the optical path length (OPL) in zone plate doesn't have to be considered. The effective transmission function T' of the zone plate looked by incident beam can be gotten by projecting zone plate to a plane which is normal to the propagation direction of incident beam, as shown in Fig. 3-5.

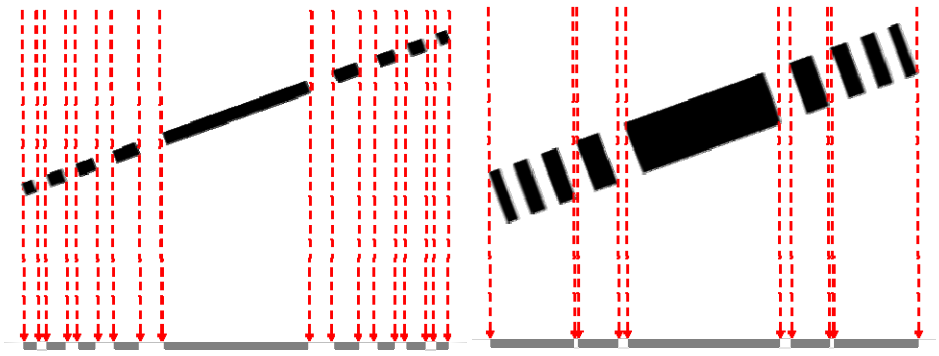

(a) (b)

Fig. 3-5 The schematic of projection of a tilted opaque zone plate. (a) The tilt angle is small. (b) If the tilt angle is too large (tilt angle $\theta \geq \tan^{-1}(\frac{1}{\text{aspect ratio}}) \cong \frac{1}{\text{aspect ratio}}$, the aspect ratio of zone plate in TXM system is about 18), the projections of the outer most zones overlap.

The relationship between the effective transmission function T' and the original transmission function T is:

$$T'(x,y) = T(x',y') \tag{3.13}$$

, where $x' = x \cdot \sec\theta$, and $y' = y$. By eq. (3.13), the effective transmission functions at different tilt angles can be calculated, and we can expect that, the focal lengths of the effective transmission function in horizontal and vertical directions will be

$$f_x' = \frac{f}{\sec^2\theta} = f\cos^2\theta \quad ,$$

$$f_y' = f \tag{3.14}$$

Since $\cos\theta \le 1$, f_x' is shorter than f .

There are the simulated projections:

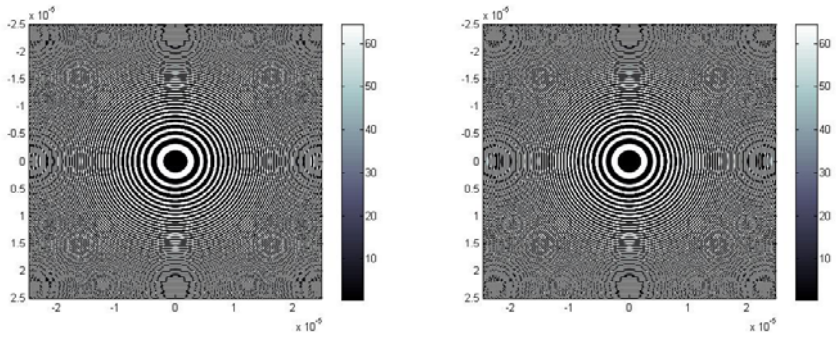

(a) (b)

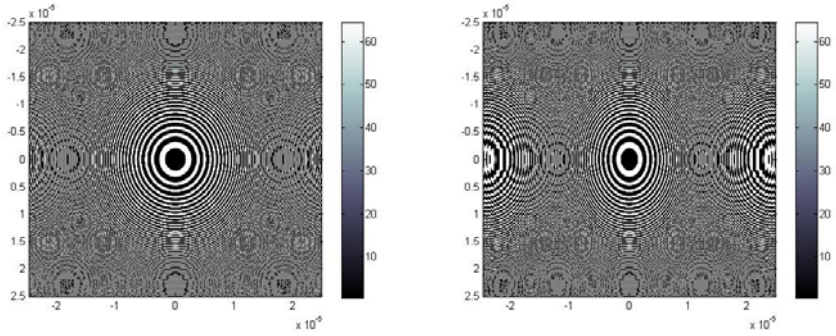

(c) (d)

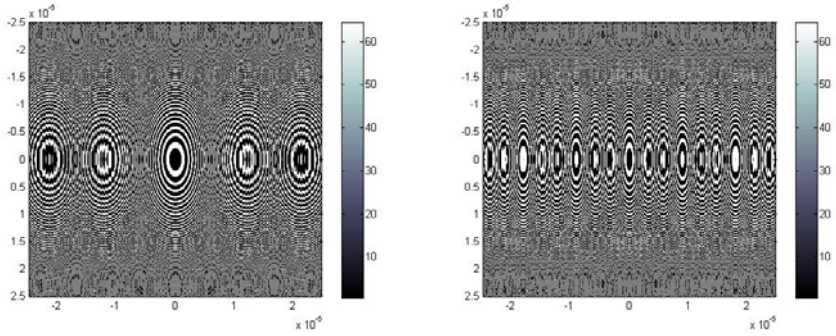

(e) (f)

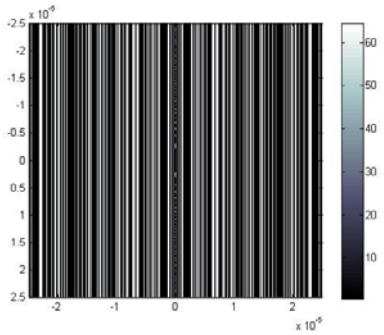

(g)

Fig.3-6 Simulation of projections of an opaque zone plate. The tilt angles in (a) to (g) are 0, 15, 30, 45, 60, 75, 90 deg., respectively. The rotation axis is y-axis.

The projections in Fig. 3-6 (b)-(g) are distorted, and not circular. The distances between those zones in horizontal direction become shorter as the tilt angle increases, so we can expect that the focal length in horizontal direction will become shorter. If the tilt angle is too large and the projections of some rings overlap, as shown in Fig. 3-5 (b), the ability to focus light in horizontal direction becomes worse.

In fact, the rings of zone plate are not completely opaque. Both the absorption and the phase shit are related to the optical path length in the zone plate. As the optical path length increases, the absorption and the phase retardation due to zone plate increase.

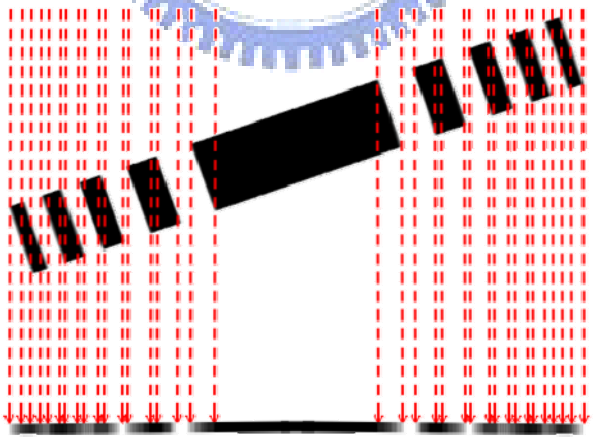

Fig. 3-7 The schematic of projection of a tilted opaque zone plate. The optical path length in zone plate has to be considered.

The optical path length in zone plate decreases gradually on the edge of rings, as shown in Fig. 3-7, so the projection is blurred on the edge. Taking the relationship between the transmission and the optical path length into account will make the

calculation of the effective transmission function to be more complicated.

In order to solve this problem, we can think the zone plate as a set of thin zone plates with transmission functions T_1, T_2, …, T_n, as shown in Fig. 3-8.

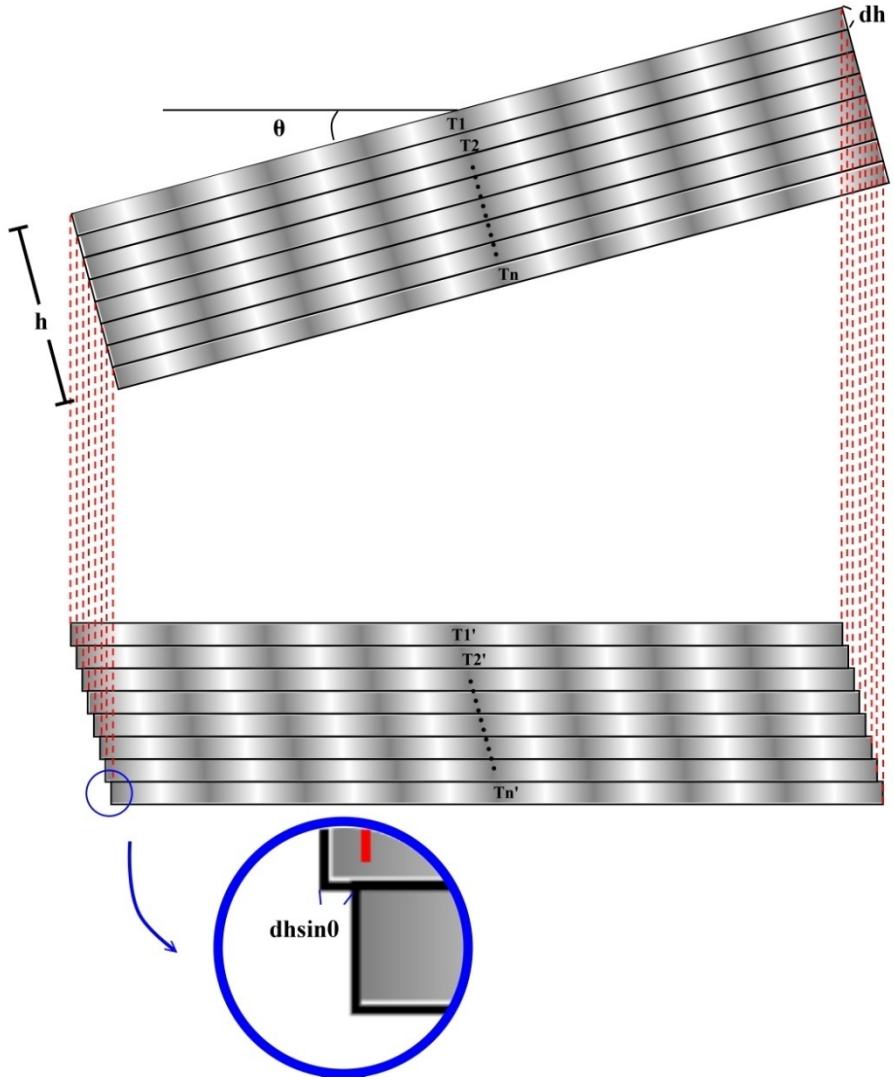

Fig. 3-8 Regard the tilted zone plate as many thin zone plates, where T_1, T_2, … T_n are the transmission functions of the thin zone plates. h is the thickness of the zone plate, and dh is the thickness of the thin zone plates. The effective transmission functions $T_1', T_2', ..., T_n'$ are the projections of T_1, T_2, … T_n, respectively. And the projections are shifted by $dh\sin\theta$ from each other.

The transmission functions of zone plate T can be expressed as:

$$T = T_1 \cdot T_2 \cdot ..... \cdot T_n = \prod_{m=1}^{n} T_m \qquad (3.15)$$

We can get the projections of those thin zone plate separately, and the effective transmission functions of the thin zone plates can be expressed as $T_1', T_2', ..., T_n'$. The relationship between T and T' is:

$$T_m'(x, y) = T_m(x', y') \tag{3.16}$$

, where m=1, 2, …., n. $x' = [x + (m - \frac{n}{2}) \cdot dh \sin\theta] \cdot \sec\theta$, and $y' = y$.

Multiple the effective transmission functions, and then we can get the effective transmission function T', ie

$$T' = T_1' \cdot T_2' \cdot ..... \cdot T_n' = \prod_{m=1}^{n} T_m' \tag{3.17}$$

By eq.(3.17), the effective transmission function of tilted zone plate can be solved, and the optical path length in zone plate v.s the radius of zone plate at different tilt angles are shown in Fig. 3-9.

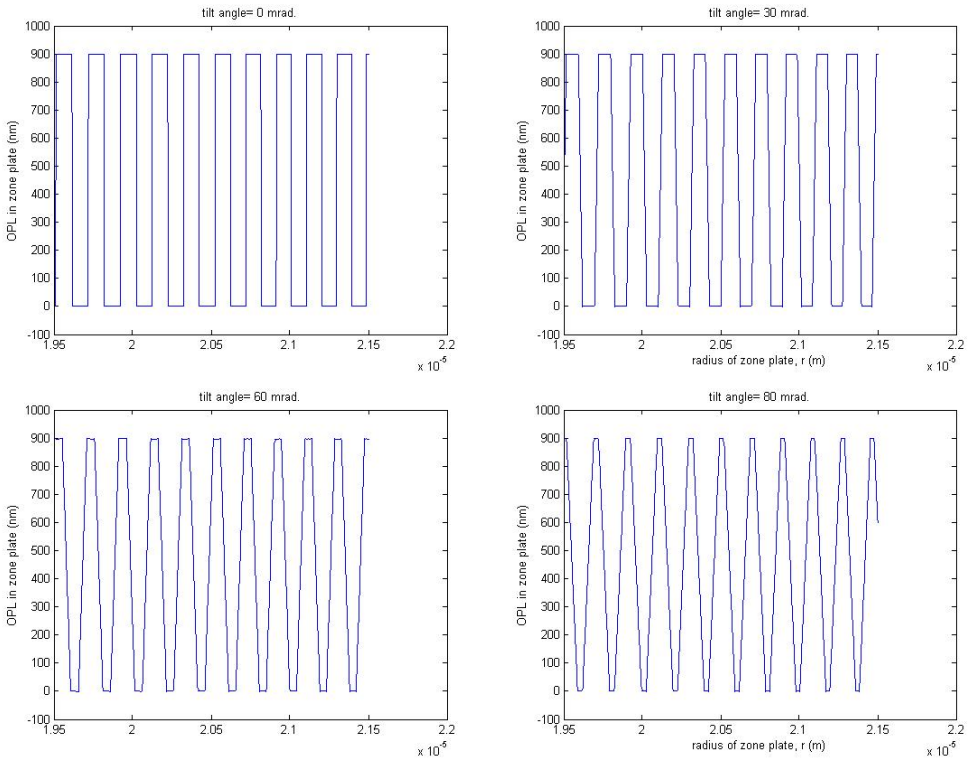

(a)

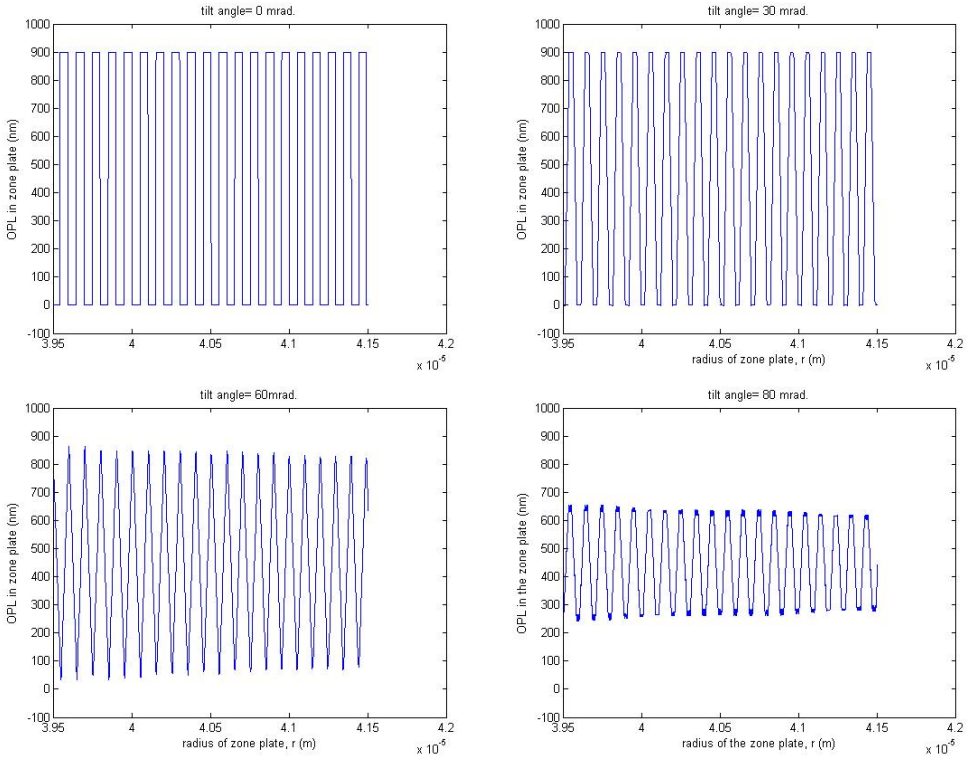

(b)

Fig. 3-9 The optical path length in zone plate v.s the radius of zone plate at different tilt angles (0, 30, 60, 80 mrad.) (a) around r=20 μ m (dr is about 100nm, the respect ratio is about 9). (b) around r=40 μ m (dr is about 50nm, the respect ratio is about 18).

In Fig. 3-9, at tilt angle $\theta = 0 mrad.$, the cross sections are composed of many rectangular functions. The edges of the cross sections become blunt when the zone plate is tilted. When the tilt angle is larger than $\tan^{-1}(\frac{1}{\text{aspect ratio}})$, the cross section is approximately triangular in shape.

3.3 Simulation Results

There are two simulation examples of zone plate tip / tilt in this section. The simulated images were obtained when the zone plate in TXM system is tipped / tilted at different angles.

Example 1:

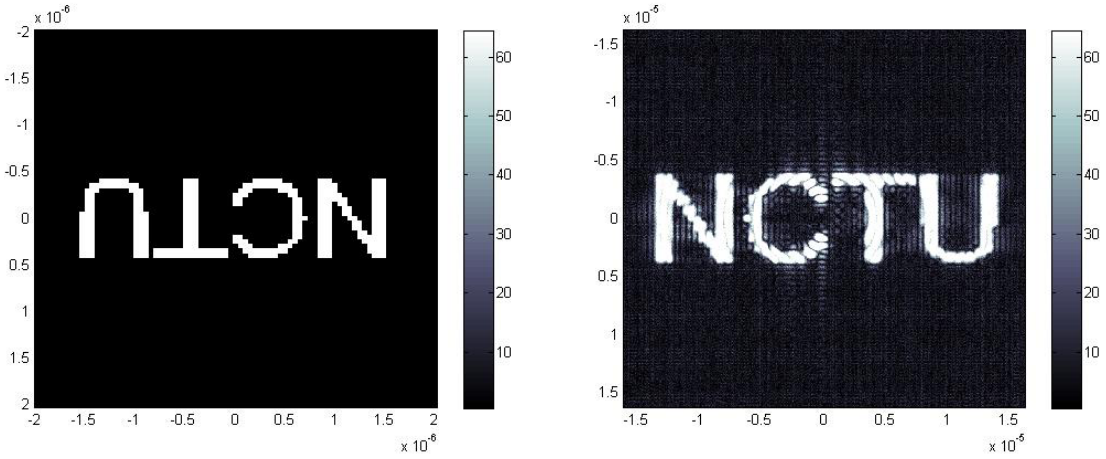

(a) (b)

Fig. 3-10 (a) The transparency of the sample which is used in this example. (b) The TXM image (the wave distribution on the image plane of the zone plate). The magnification is 9.

In order to find out the position of circle of least confusion, focal series of images were gotten by simulation. The best image of the series of images at each tip / tilt angle is shown in Table 3-1:

	0 mrad.	10 mrad.	20 mrad.
Tip	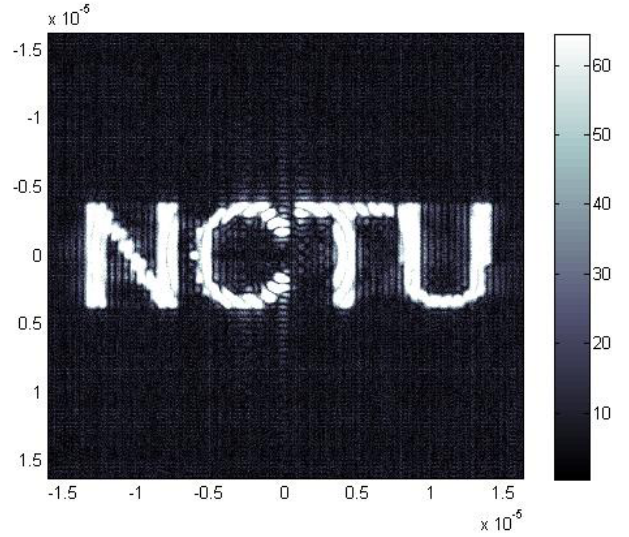	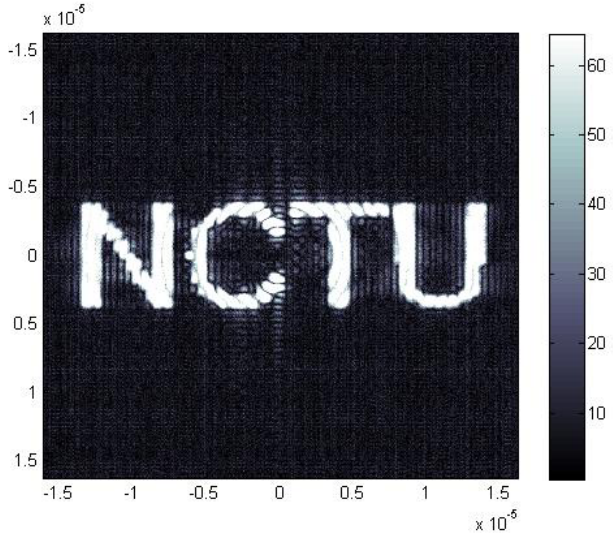	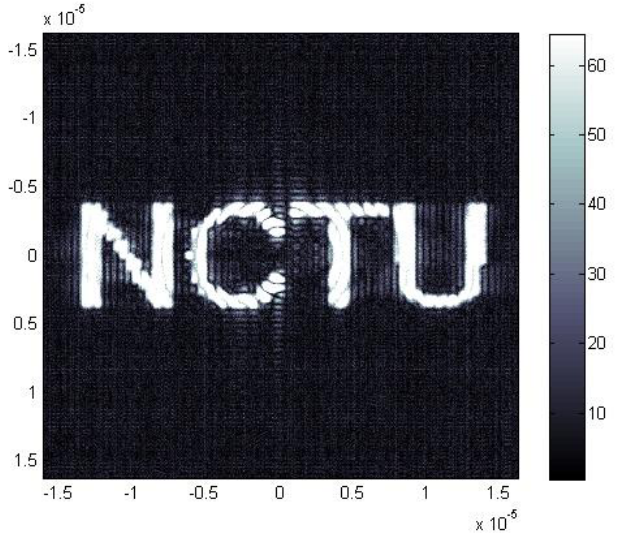
Tilt	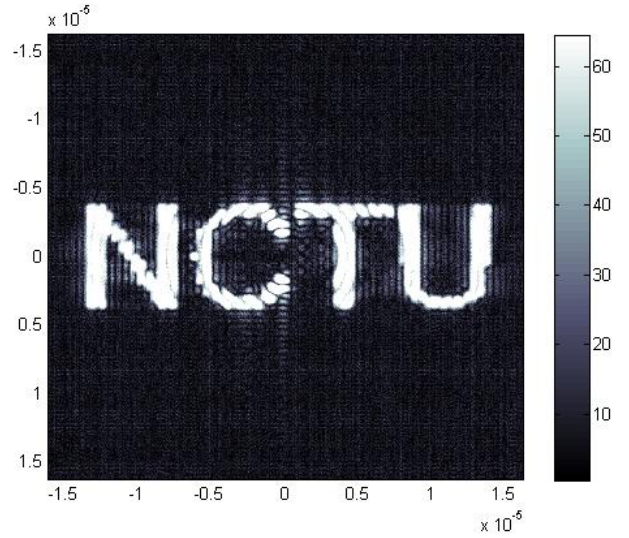	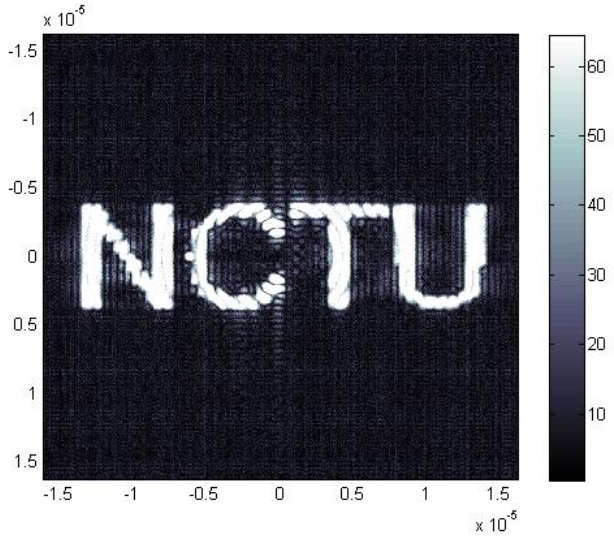	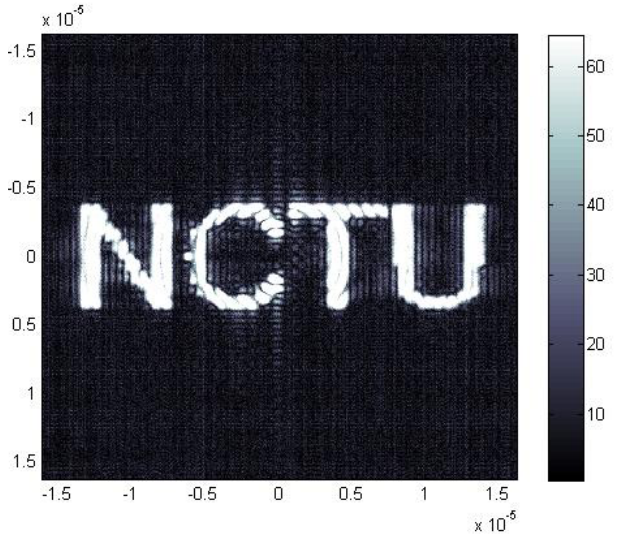

Table 3-1 (a) The simulated images are gotten when the zone plate is tipped /tilted by 0, 10, 20 mrad.

	30 mrad.	40 mrad.	50 mrad.
Tip	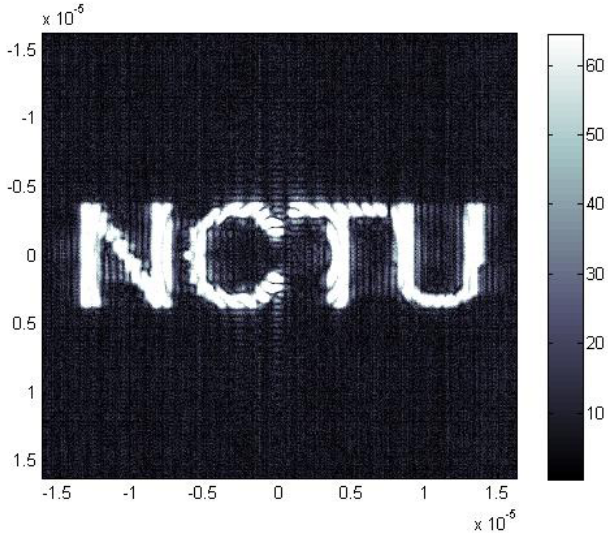	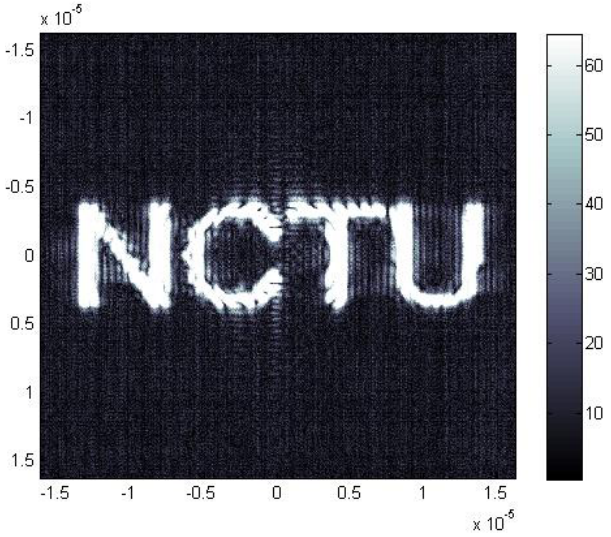	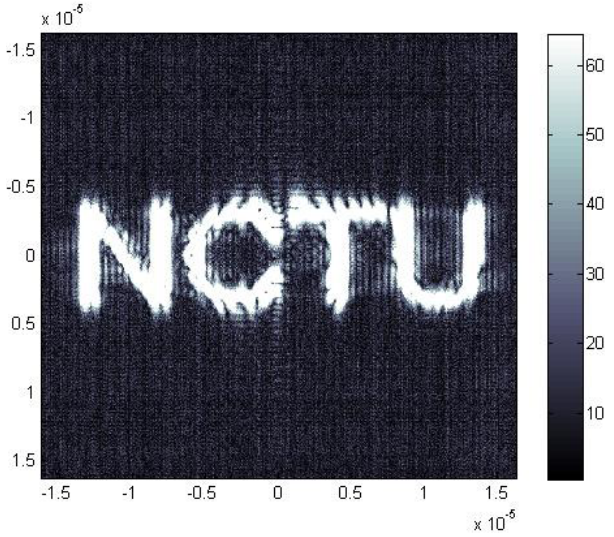
Tilt	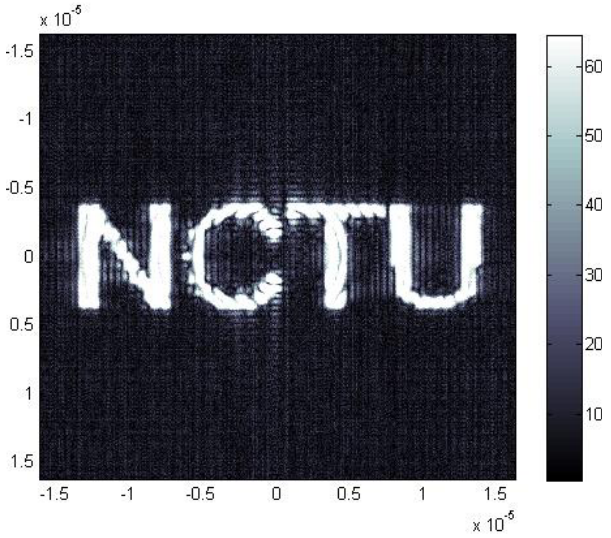	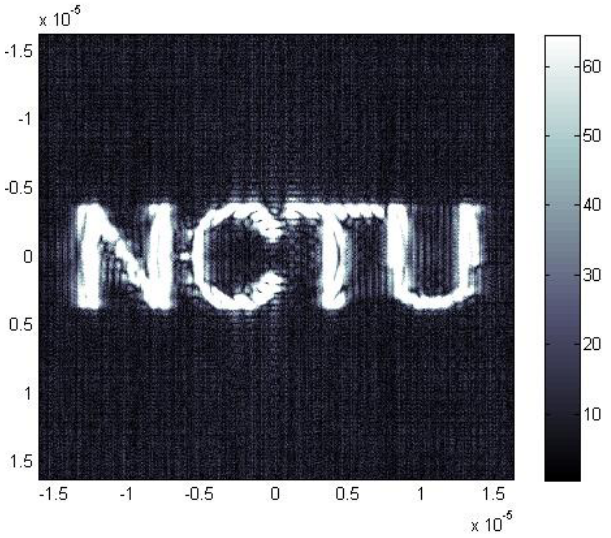	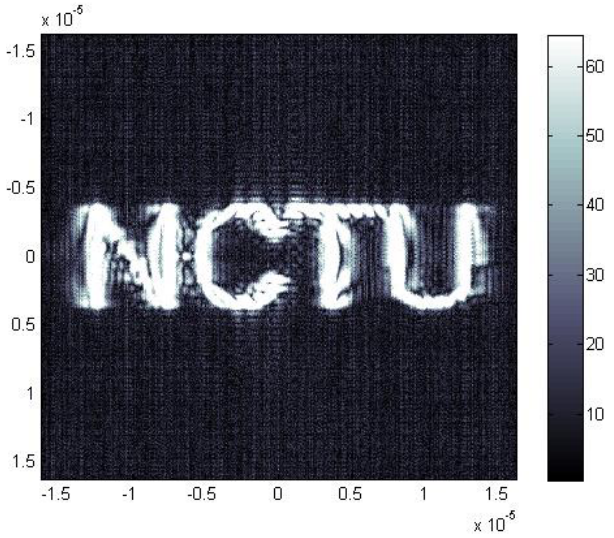

Table 3-1 (b) The simulated images are gotten when the zone plate is tipped /tilted by 30, 40, 50 mrad.

	60 mrad.	70 mrad.	80 mrad.
Tip	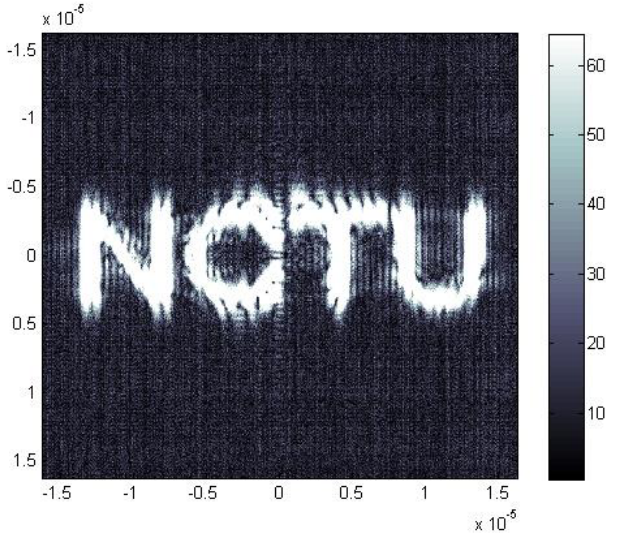	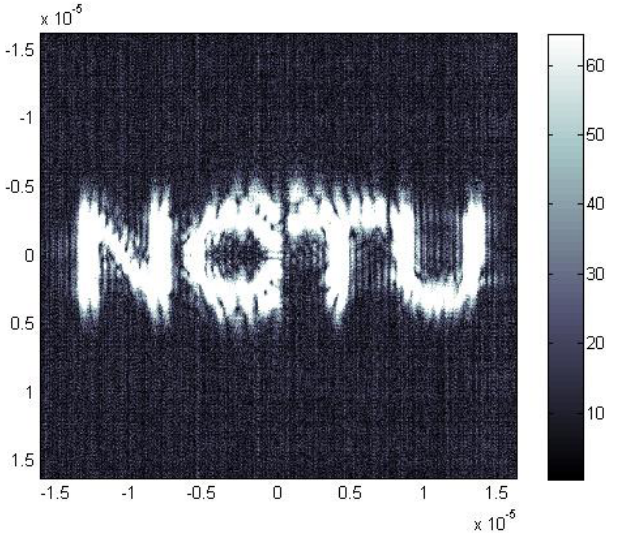	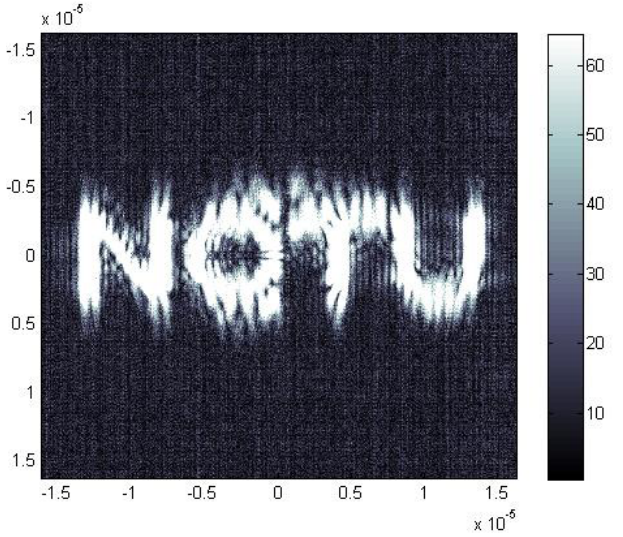
Tilt	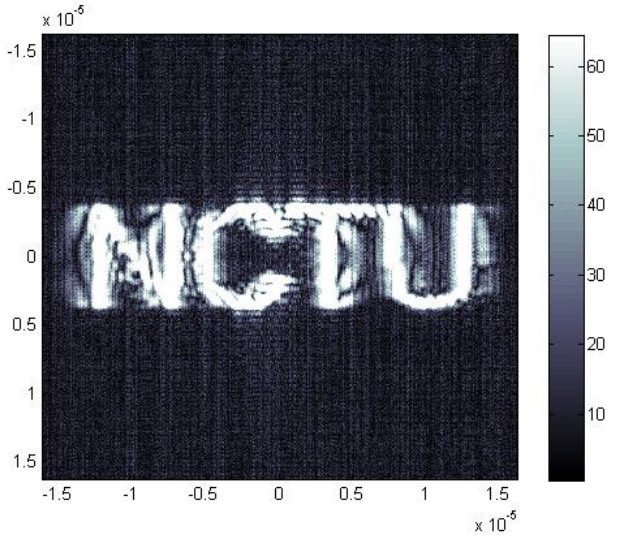	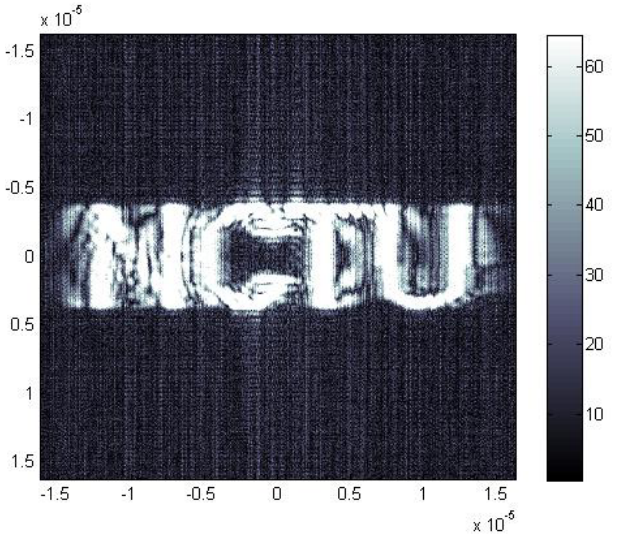	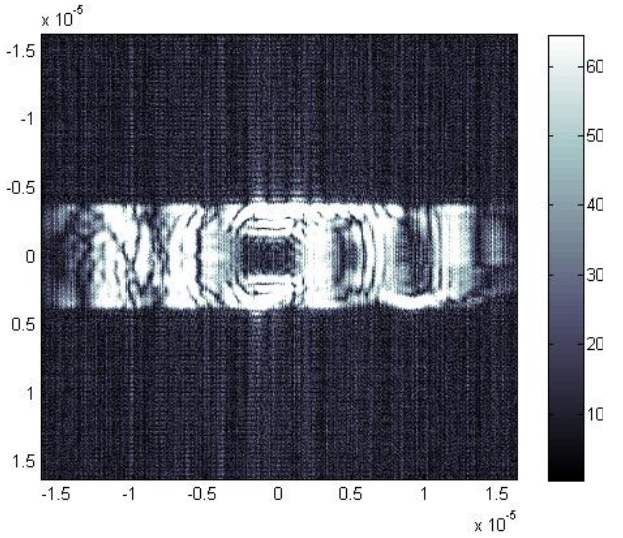

Table 3-1 (c) The simulated images are gotten when the zone plate is tipped /tilted by 60, 70, 80 mrad.

Compare Fig. 3-10 (b) with the images in Table 3-1, we can see that, the images will be stretched in vertical direction when the zone plate is tipped, and they will be compressed in horizontal direction when the zone plate is tilted. Besides, when the tip / tilt angle of zone plate is larger than 50 mrad., the TXM image will be evidently distorted.

Example 2:

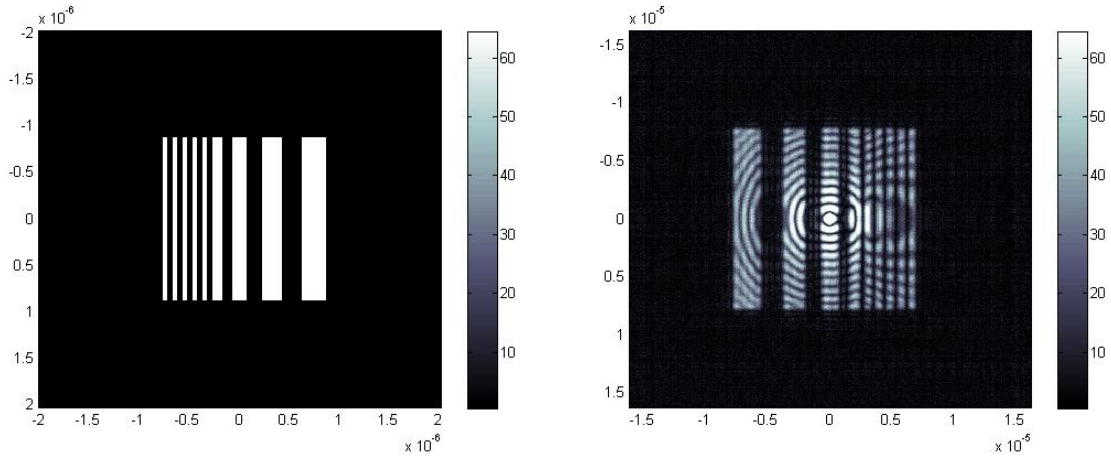

Fig. 3-11 (a) The transparency of the test sample. There are 9 vertical lines, the width of the thinnest line is 50nm. (b) The TXM image. The magnification is 9.

The simulated images are shown in Table 3-2:

	0 mrad.	10 mrad.	20 mrad.
Tip	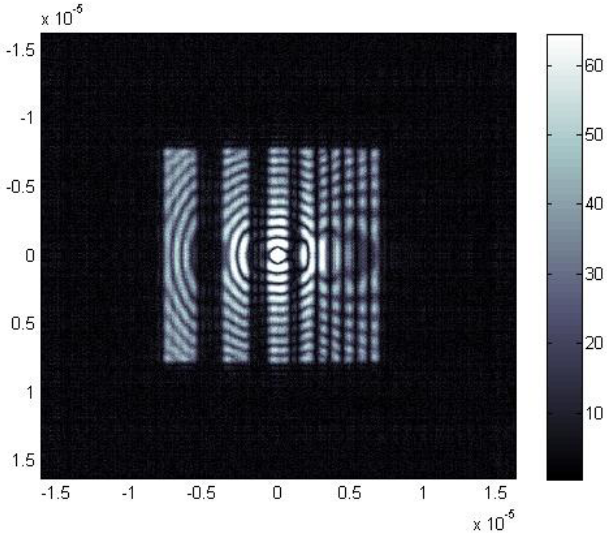	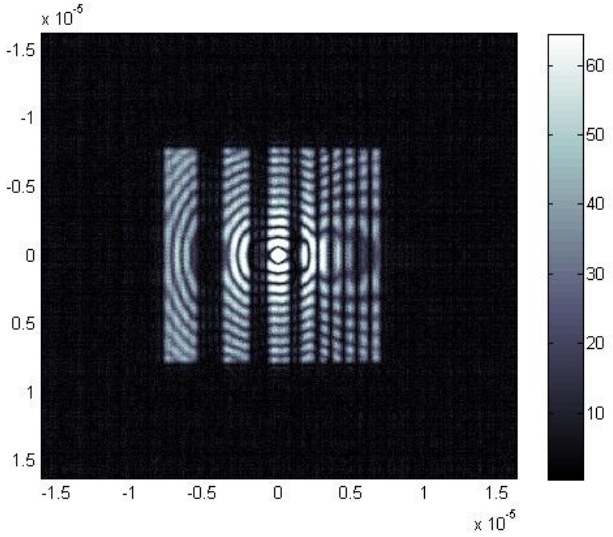	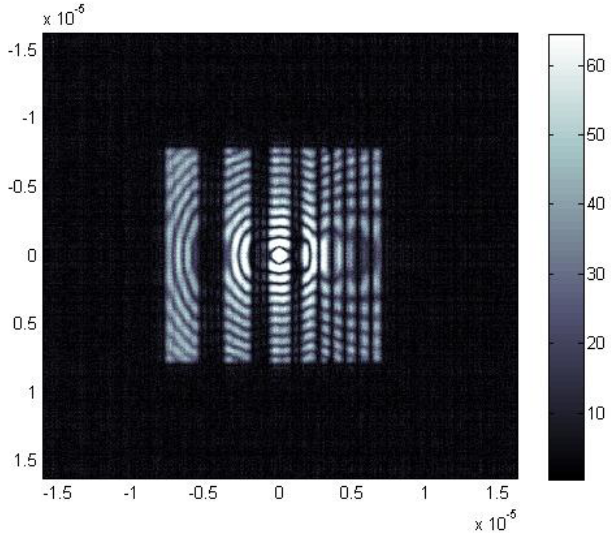
Tilt	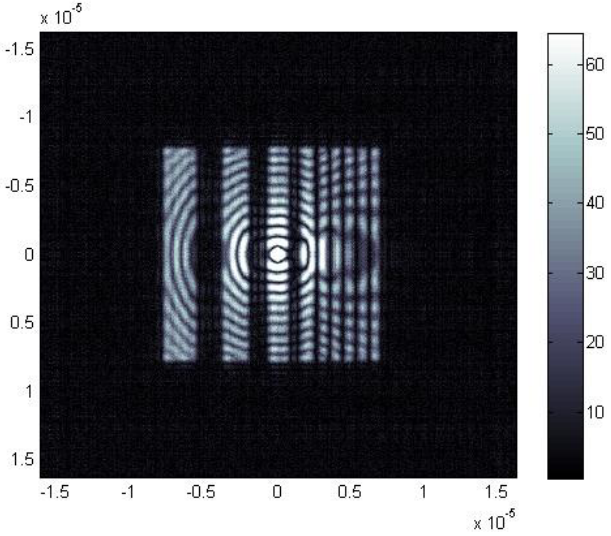	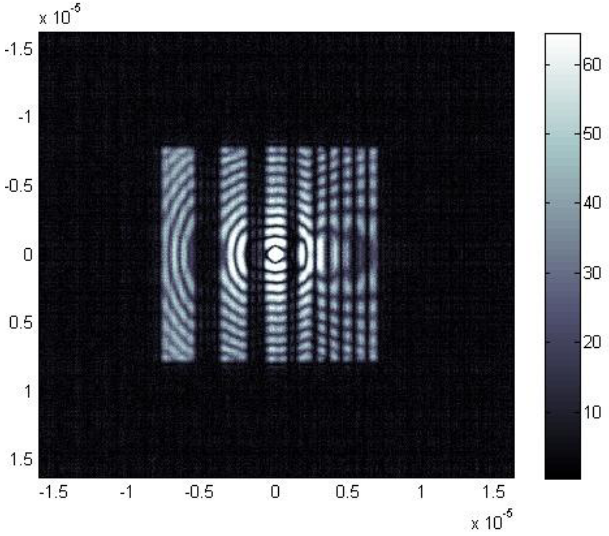	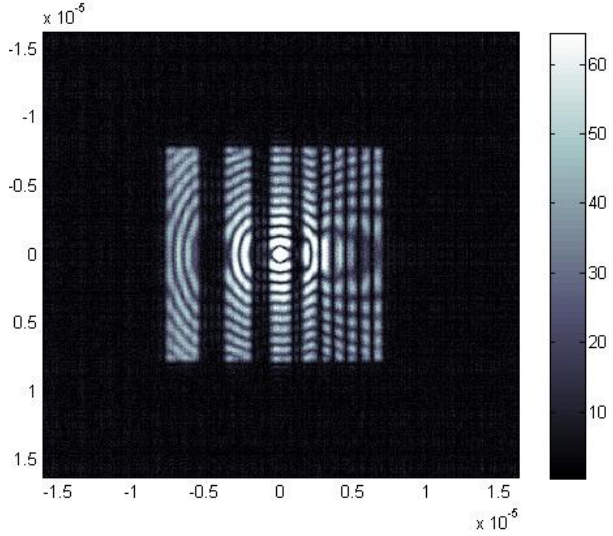

Table 3-2 (a) The simulated images are gotten when the zone plate is tipped /tilted by 0, 10, 20 mrad.

	30 mrad.	40 mrad.	50 mrad.
Tip	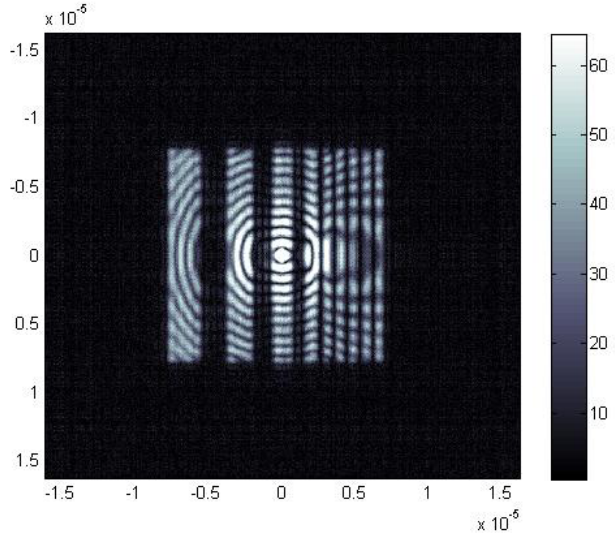	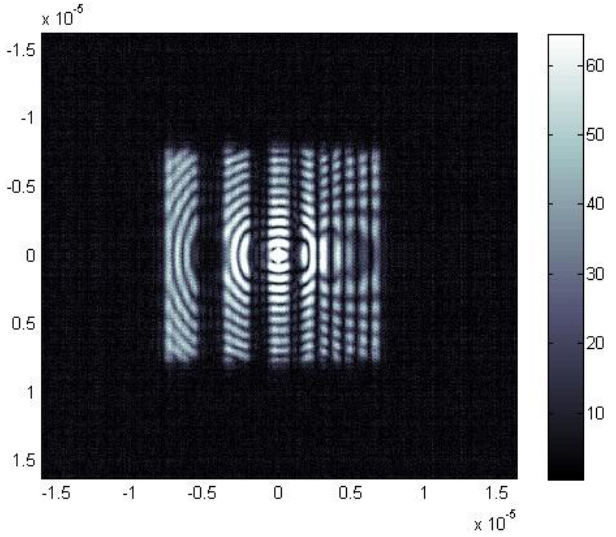	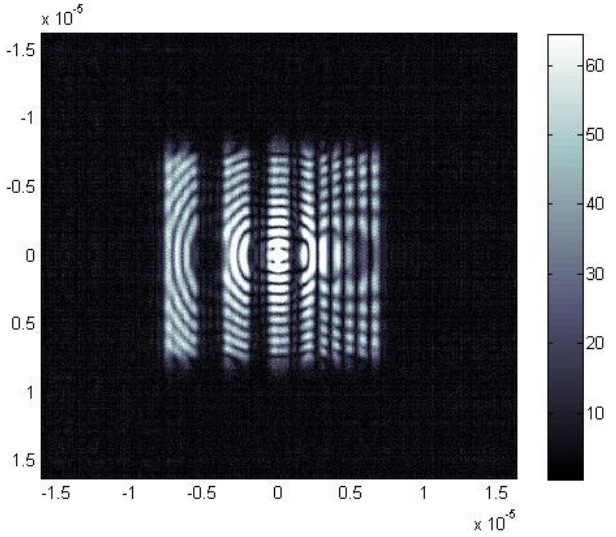
Tilt	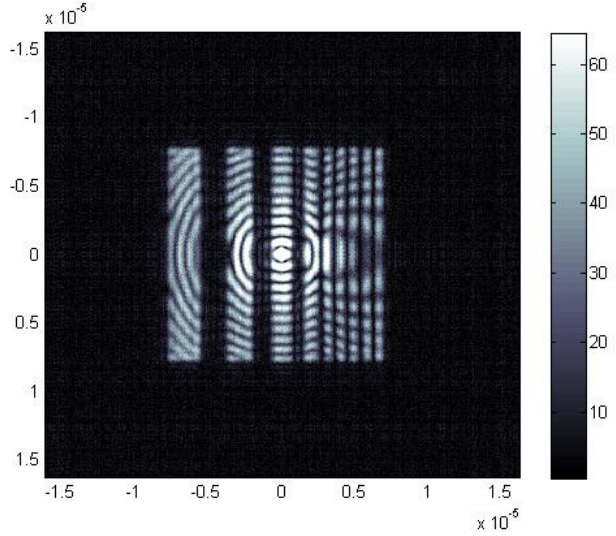	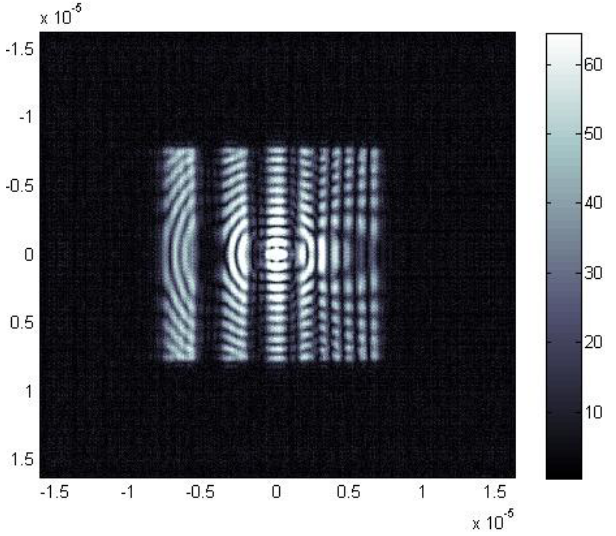	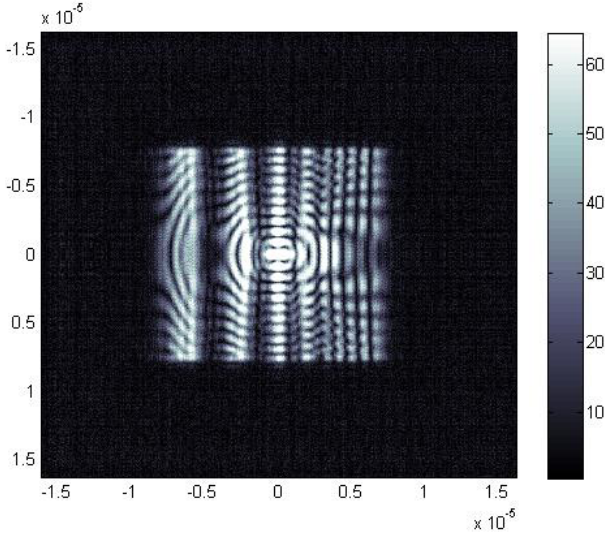

Table 3-2 (b) The simulated images are gotten when the zone plate is tipped /tilted by 30, 40, 50 mrad.

	60 mrad.	70 mrad.	80 mrad.
Tip	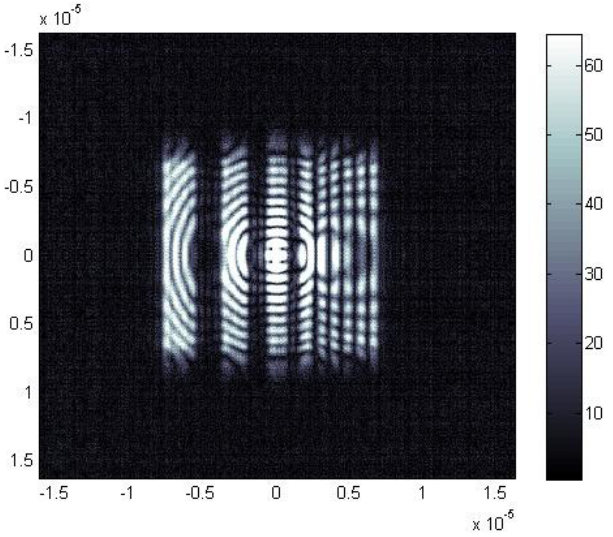	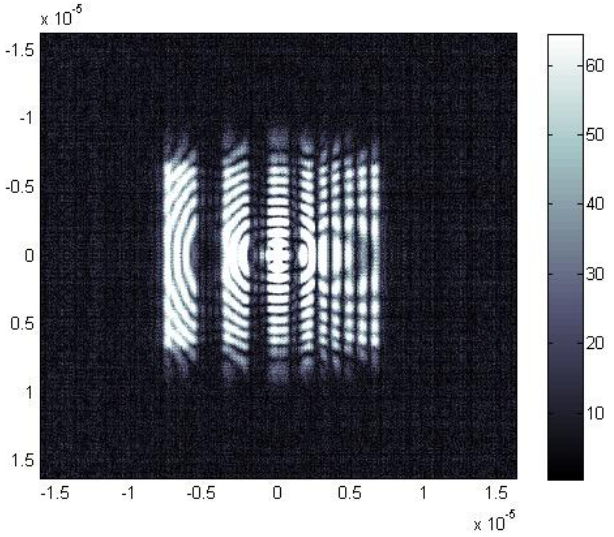	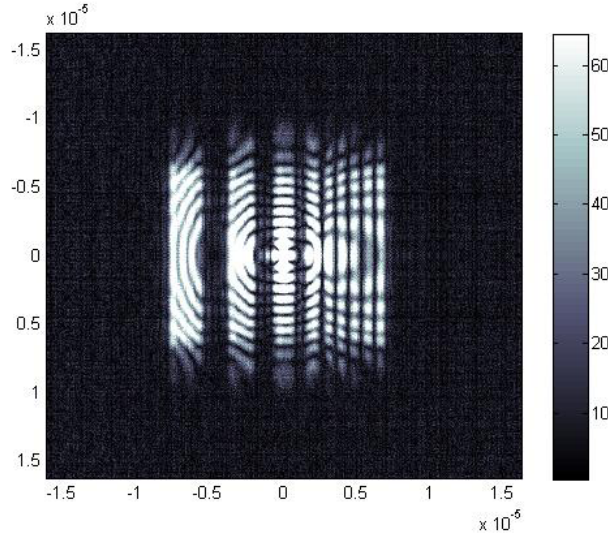
Tilt	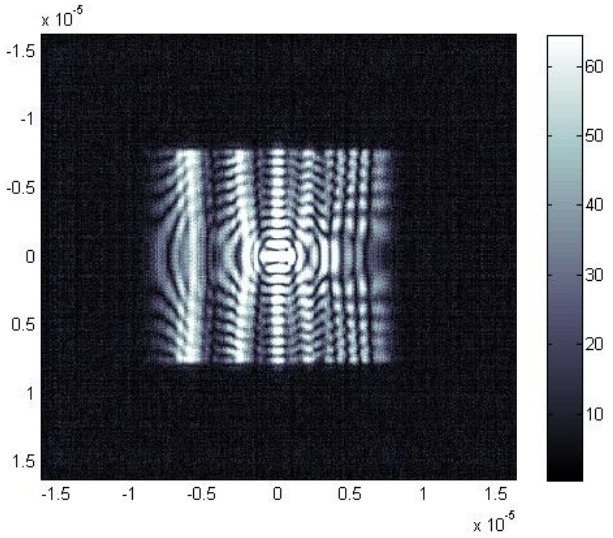	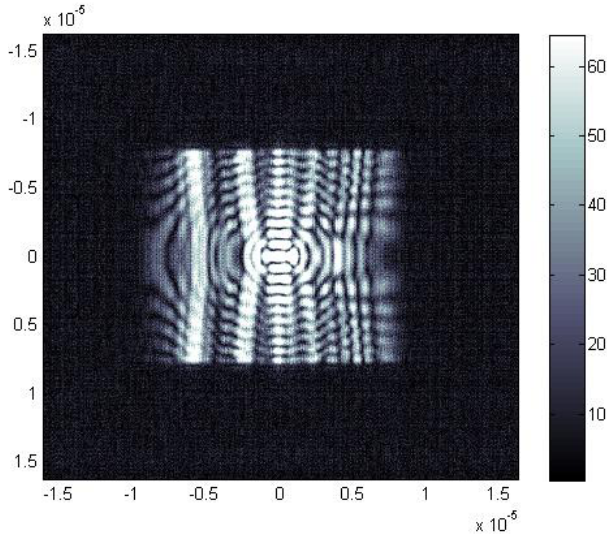	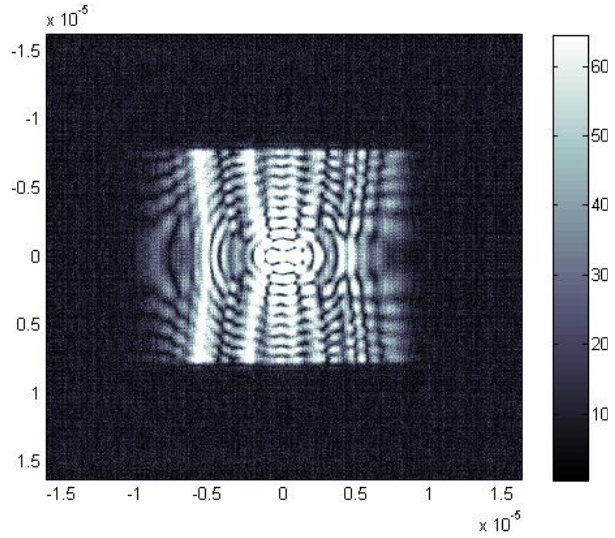

Table 3-2 (c) The simulated images are gotten when the zone plate is tipped /tilted by 60, 70, 80 mrad.

Compare Fig. 3-10 (b) with the images in Table 3-2, we can see that, the simulated TXM images are distorted and blurred when the zone plate is tipped / tilted. And the edges of the patterns are blurred, the contrasts become worse.

3.4 Analysis

In this section, the simulation results of the example 2 in previous section will be analyzed and discussed.

According to the line amplitude plots of the images, the images is affected by zone plate tip / tilt in x and y directions. (The line amplitude plot of U_6 on the line $x=x_0$ is $U_6(x_0,y)$). Judging by the line plot at fixed x or y is not adequate, since the amplitude distribution of U_6 is also affected by the wave distribution of incident beam, and the amplitude of the incident beam at the center is much larger. In order to get the statistical data, we integrated the wave function U_6 in y and x directions, and the normalized results are defined as C(x) and C(y), where

$$C(x) \equiv \frac{\int_{y1}^{y2} |U_6(x,y)|\,dy}{[\int_{y1}^{y2} |U_6(x,y)dy|]_{max}}, \quad C(y) \equiv \frac{\int_{x1}^{x2} |U_6(x,y)|\,dx}{[\int_{x1}^{x2} |U_6(x,y)dx|]_{max}} \tag{3.18}$$

Since the simulated wave function U_6 in Matlab is a discrete matrix, we calculate the summation of matrix $|U_6|$ instead of calculating the integration of wave function $|U_6|$, as shown in Fig. 3-11. Eq. (3.18) can be rewritten as:

$$Cx \equiv \left(\frac{\sum_{i=m}^{n} |U_{6\,i,j}|}{[\sum_{i=m}^{n} |U_{6\,i,j}|]_{max}}\right)_{j=m,m+1,\ldots,n}, \quad Cy \equiv \left(\frac{\sum_{j=m}^{n} |U_{6\,i,j}|}{[\sum_{j=m}^{n} |U_{6\,i,j}|]_{max}}\right)_{i=m,m+1,\ldots,n} \tag{3.19}$$

, where Cx and Cy are arrays. (For our simulation, U_6 is a 2601×2601 matrix, the distance between each pixel is 50 nm, and we chose m=900, n=1700.)

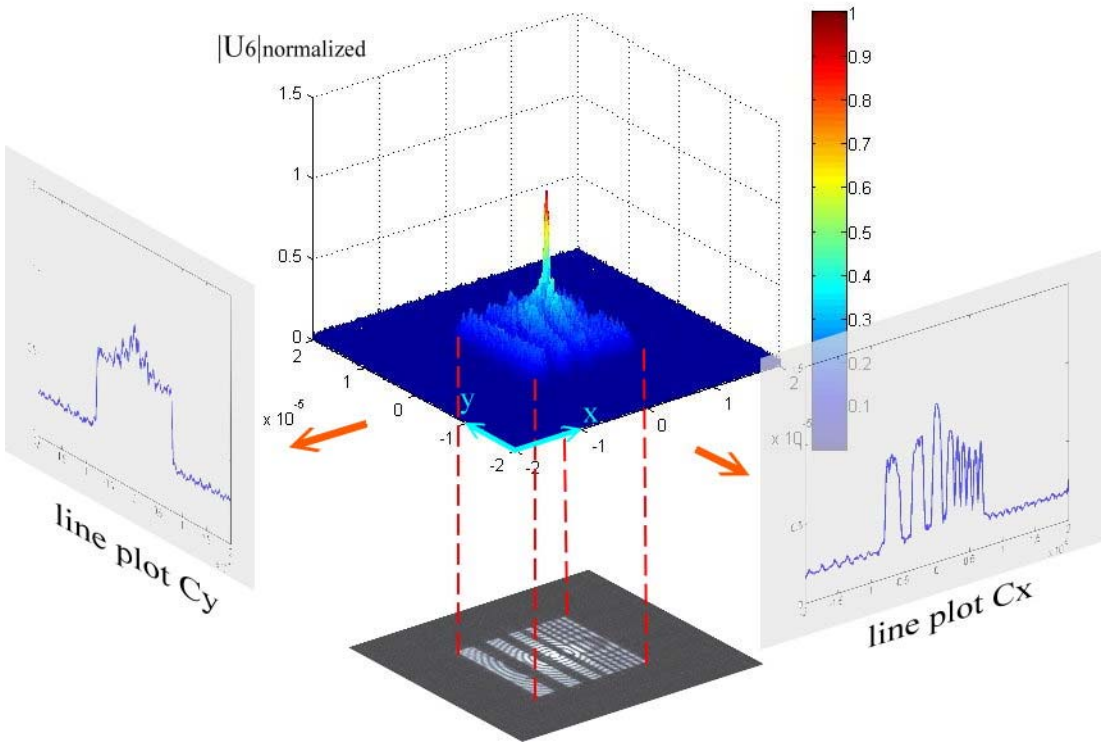

Fig. 3-12 The line plot Cx / Cy is the sum of the m^{th} to nth rows / columns of matrix |U6|.

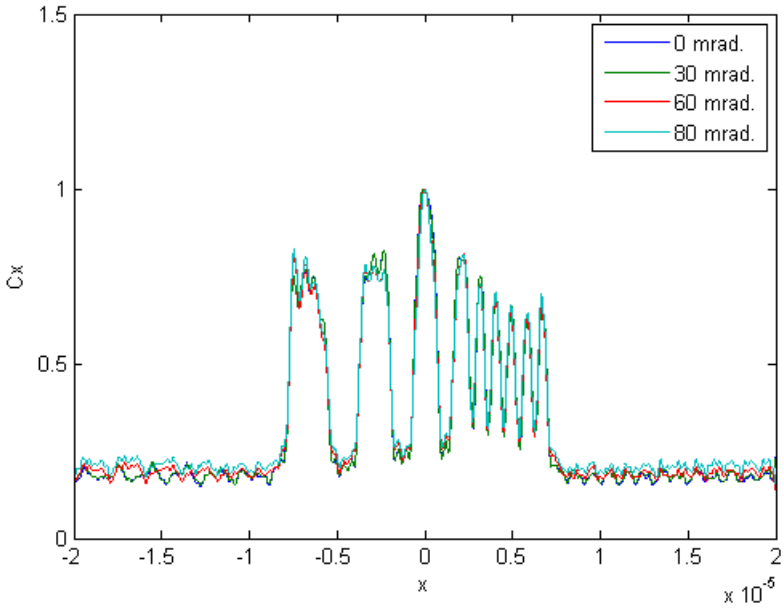

(a)

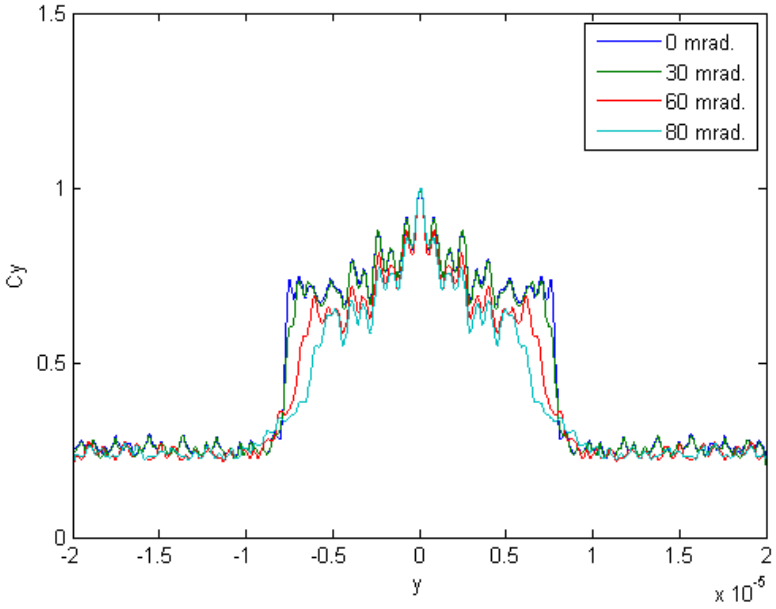
0 mrad.
30 mrad.
60 mrad.
80 mrad.
Cy
y
x 10^-5

(b)

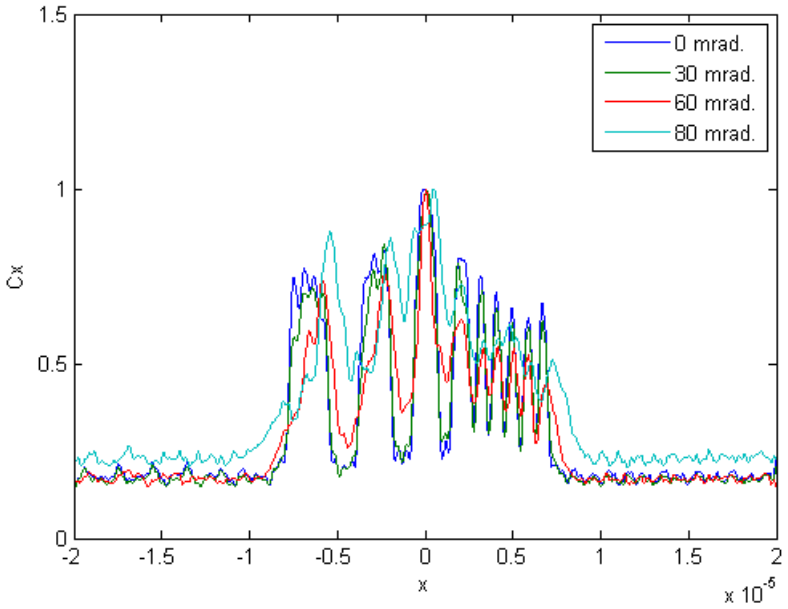
0 mrad.
30 mrad.
60 mrad.
80 mrad.
Cx
x
x 10^-5

(c)

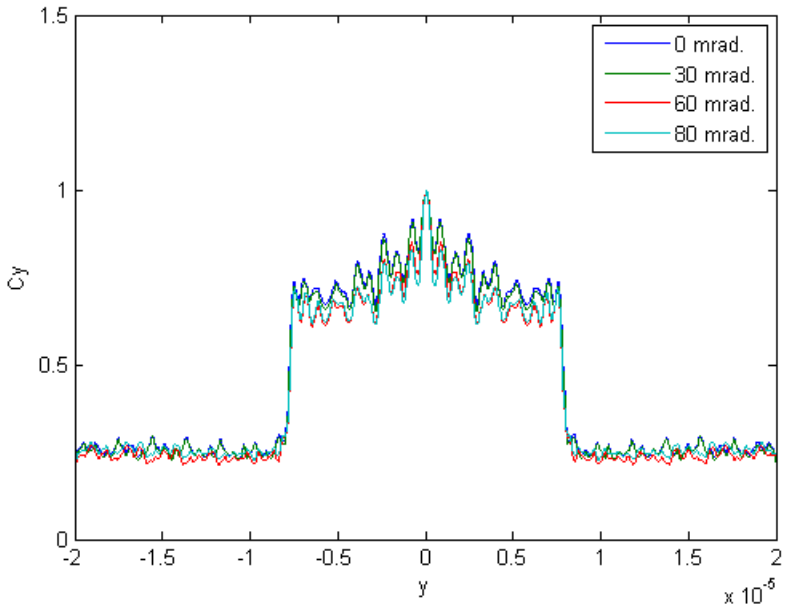

(d)

Fig. 3-13 (a) shows the line plots Cx, and (b) shows the line plots Cy of images obtained when the zone plate is tipped by 0, 30, 60, and 80 mrad. (c) shows the line plots Cx, and (d) shows the line plots Cy when the zone plate is tilted by 0, 30, 60, and 80 mrad.

The line plots of different tip / tilt angles are almost the same in Fig. 3-13 (a) / (d). That is, the amplitude distributions of U_6 in x / y direction won't change evidently when the zone plate is tipped / tilted. However, the line plots of different tip / tilt angles in Fig. 3-13 (b) / (c) are quite different. In Fig. 3-13 (b) and (c), the edges of the pattern get blunter, and the contrasts become worse as the tip / tilt angle increases.

The contrast modulation is defined as:

$$\text{Contrast modulation} \equiv \frac{C_{maximum} - C_{minimum}}{C_{maximum} + C_{minimum}} \qquad (3.19)$$

Compare Fig. 3-13 (a) and (c), and calculate the contrast modulations. The relationships between the contrast modulations in Fig. 3-13 (a), (c) and the tip / tilt angles are shown in Fig. 3-14.

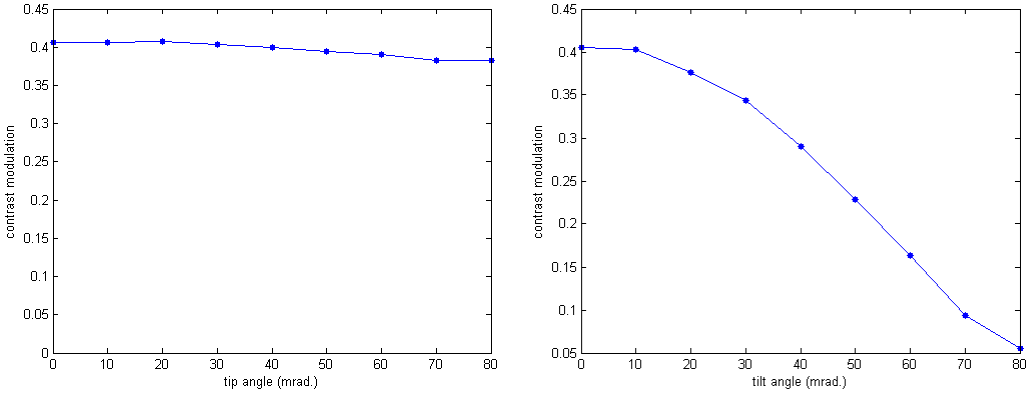

(a) (b)

Fig. 3-14 (a) Contrast modulation v.s tip angle, and (b) contrast modulation v.s tip angle at spatial frequency $\nu = \frac{1}{50nm} = 20\text{MHz}$.

By Fig. 3-13, we can see that, the contrast modulation of TXM image doesn't change obviously as the tip angle increases. Nevertheless, the contrast modulation decreases as the tilt angle increases.

3.5 Summary

According to section 3.2, the focal lengths f_x and f_y of a tipped / tilted zone plate are not the same, and astigmatism will occur. Additionally, when the tip / tilt angle is larger than the reciprocal of zone plate's aspect ratio, the ability to focus light in vertical / horizontal direction of the zone plate will be much worse. In this chapter, the TXM images with zone plate tip / tilt are simulated by Matlab. By the simulation results and the analysis in previous sections, zone plate tip / tilt affect the image quality (Zone plate tip / tilt distort the shape of simulated image and make the contrast modulation decrease). The experimental results will be shown in chapter 4, and the experimental and simulation results will be compared.

Chapter 4
Experimental Results

In chapter 3, the TXM images with different tip / tilt angles were obtained by simulation. The experimental results of zone plate tilt in TXM system will be shown in this chapter.

4.1 The Experiment of Zone Plate Tilt

4.1.1 Five Axes Stage in TXM System

In TXM system, the zone plate holder is put on a five axes stage. The stage was designed and manufactured by Newport company, called AG-M050, as an optical mount, as shown below in Fig. 4-1. It can move zone plate in x, y, and z directions, tip and tilt zone plate (The angular range of AG-M050 is about ± 2 deg. $\cong \pm 34.9$ mrad., the maximum tip / tilt angle of our five axes stage is about 40 mrad.). There is a piezoelectric crystal in the stage to adjust the tip / tilt angle. Experiments of zone plate tilt can be done with this stage.

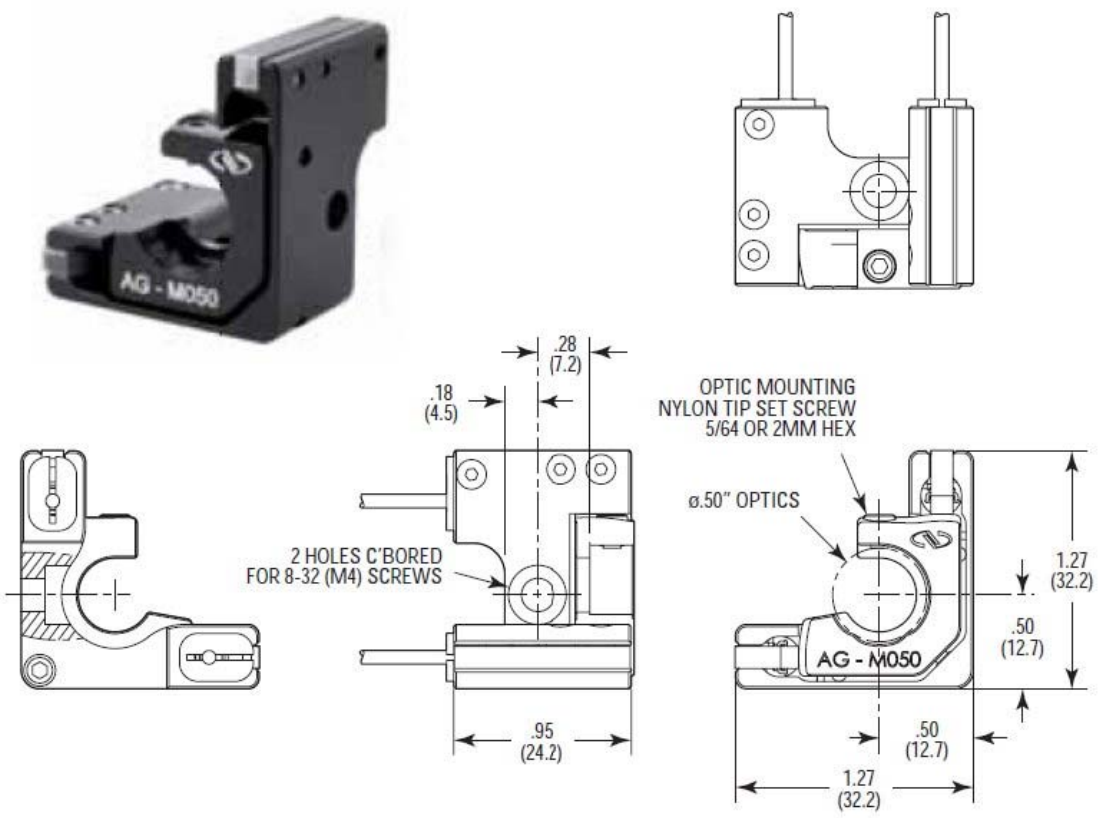

(a)

(b)

Fig. 4-1 (a) Model AG-M050. (b) Five axes stage of the zone plate holder in TXM system.

4.1.2 The Siemens Star

The Siemens star is also called the spoke pattern and it is a device to test the resolution of optical instruments. This pattern is made by Yu-Tong Chen (Ref[10]).The line width of the spoke pattern is narrower in the inner part than in the outer part. A spoke pattern was used to be the test sample in the zone plate tip / tilt experiment.

For the Siemens star which was used in our experiment, the width of the pattern in each zone was between 40 nm to 50 nm, 50 nm to 60 nm, 60 nm to 70 nm, 70 nm to 80 nm, 80 nm to 90 nm, 90 nm to 100 nm (from the inner most zone to the out most zone). Fig. 4-2 shows the TXM image of the Siemens star which was obtained without tilting the zone plate:

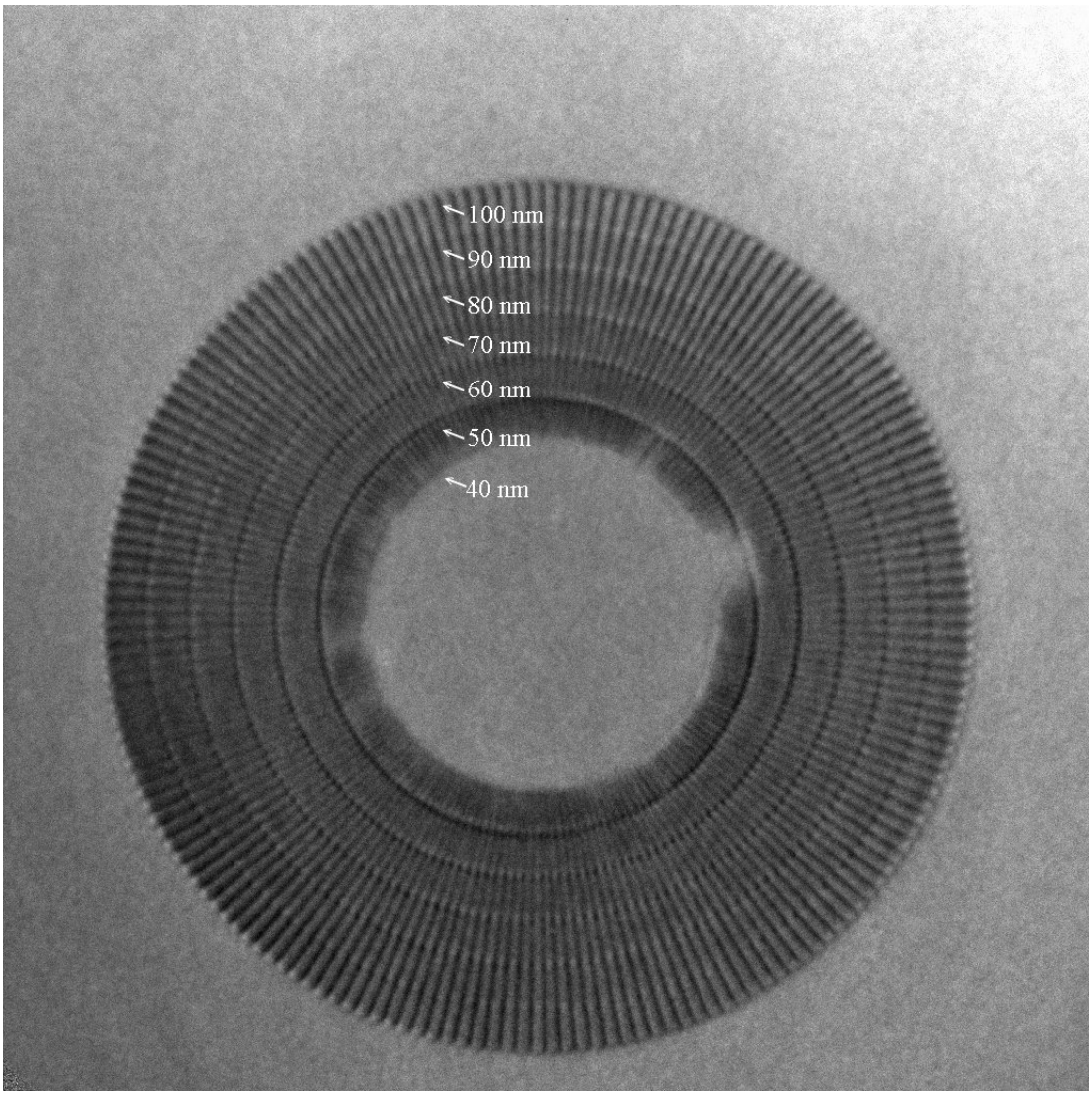

Fig. 4-2 The TXM image of the Siemens star.

4.2 Experimental Data and Line Plots

The experimental results are shown in Table 4.1:

	TXM image	Line plots
Tilt angle =0mrad	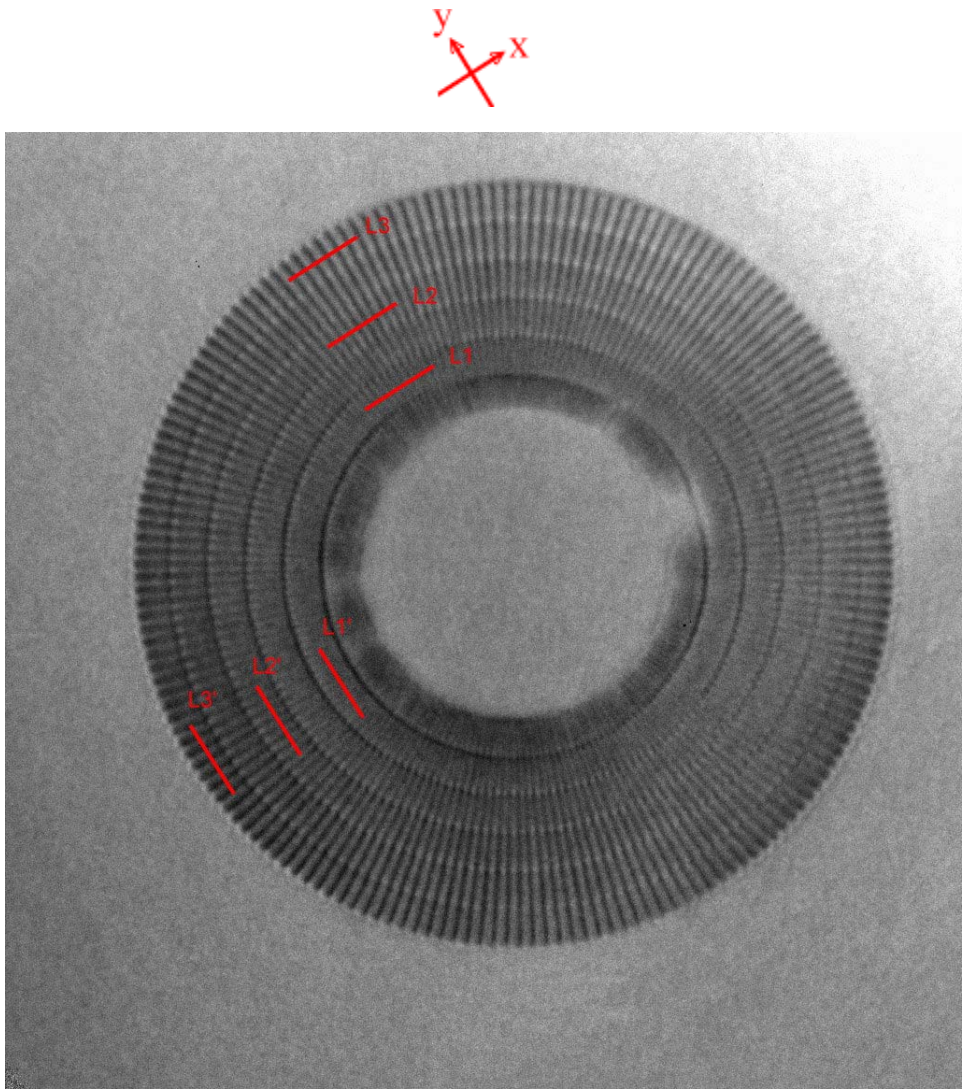	(i) 50~60 nm 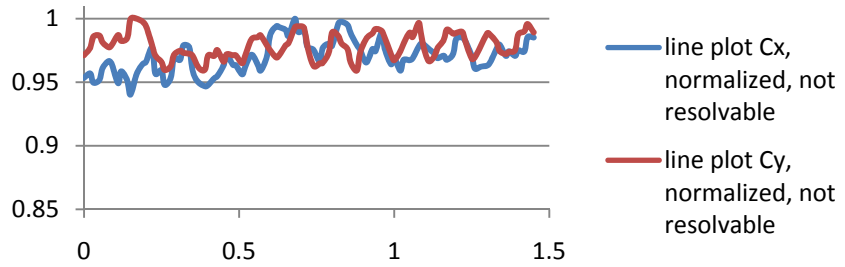 (ii) 70~80 nm 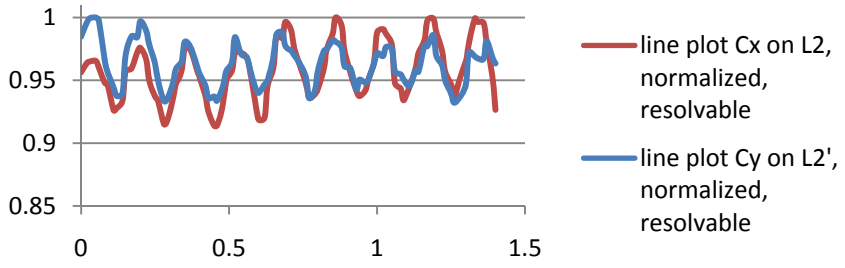 (iii) 90~100 nm 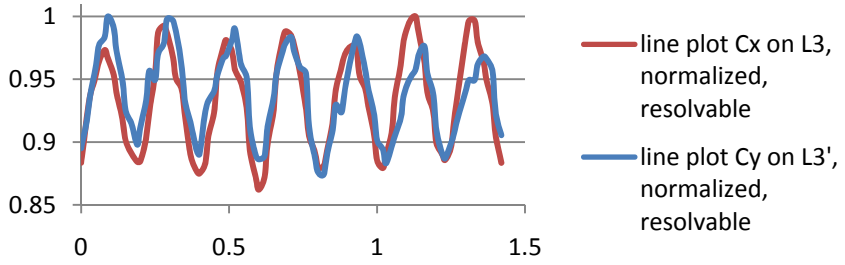

Table 4-1 (a) TXM image and the line plots at tilt angle = 0 mrad. The line plots were drawn on (i) line L1, and line L1’ in the second zone (50~60 nm), (ii) line L2, and line L2’ in the forth zone (70~80 nm), (iii) line L3, and line L3’ in the outmost zone (90~100nm).

	TXM image	Line plots
Tilt angle =10mrad	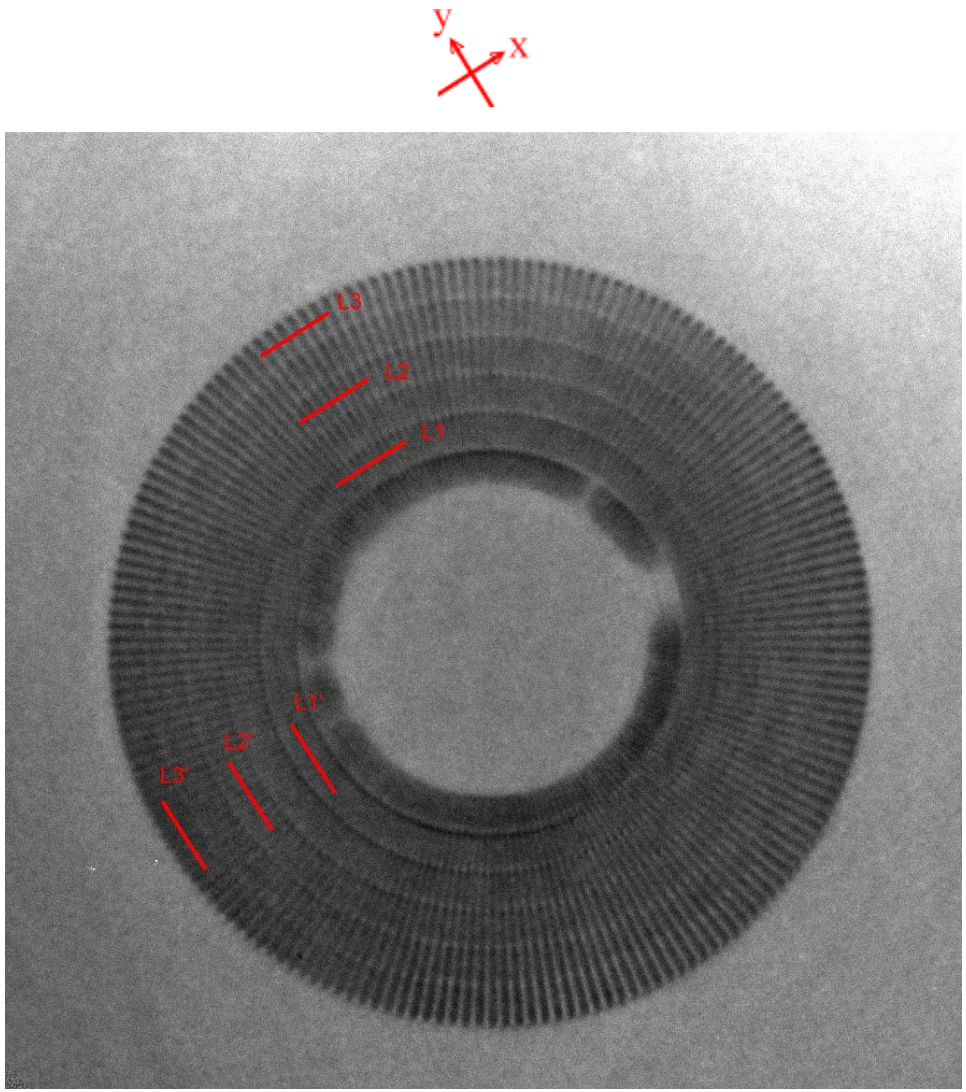	(i) 50~60 nm 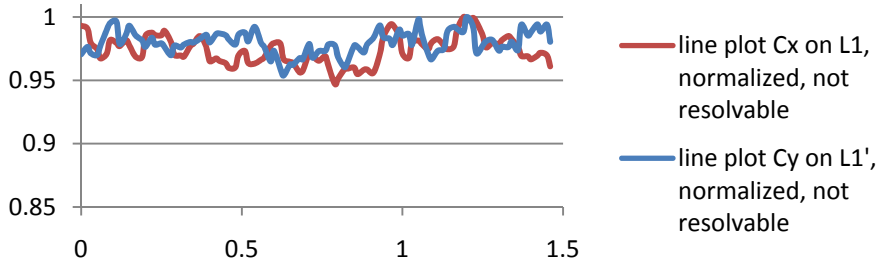 (ii) 70~80 nm 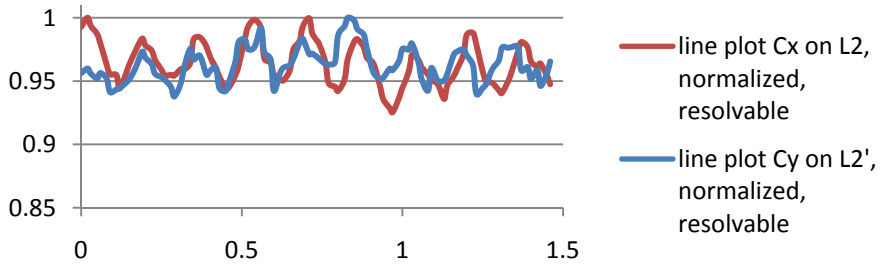 (iii) 90~100 nm 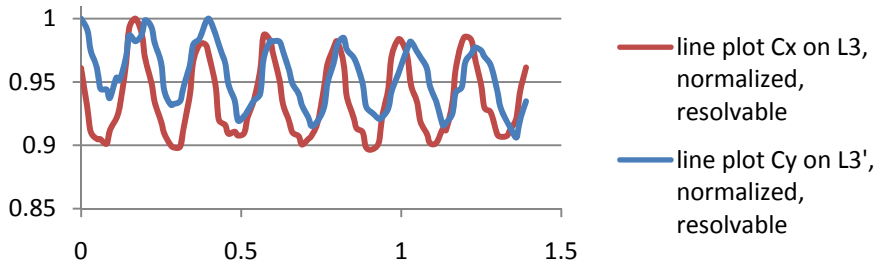

Table 4-1 (b) TXM image and the line plots at tilt angle = 10 mrad. The line plots were drawn on (i) line L1, and line L1’ in the second zone (50~60 nm), (ii) line L2, and line L2’ in the forth zone (70~80 nm), (iii) line L3, and line L3’ in the outmost zone (90~100nm).

	TXM image	Line plots
Tilt angle =20mrad	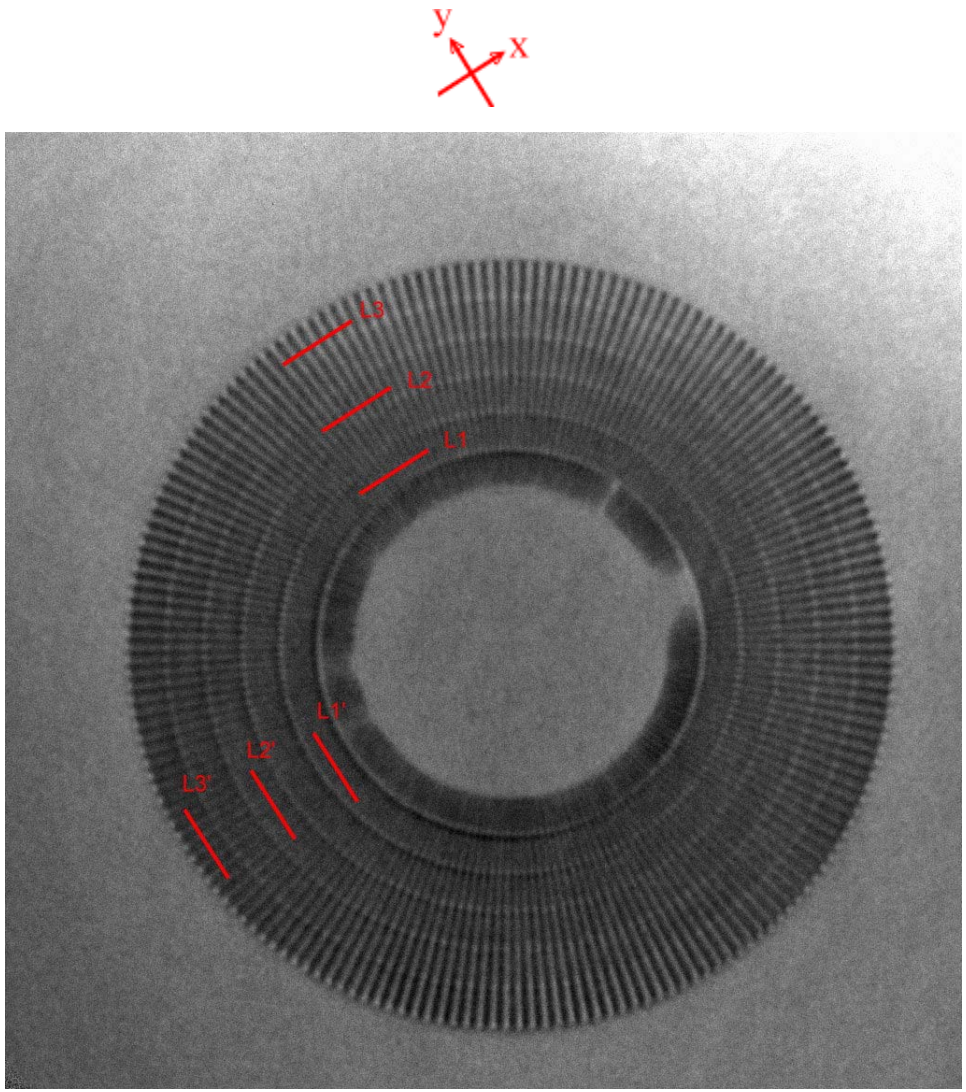	(i) 50~60 nm 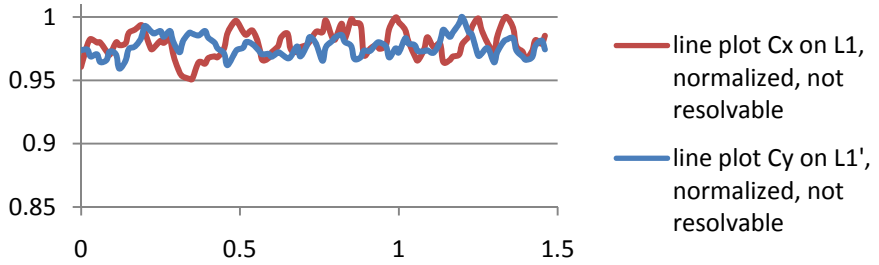 (ii) 70~80 nm 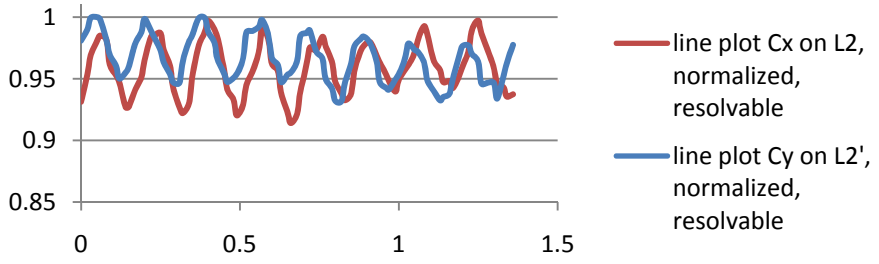 (iii) 90~100 nm 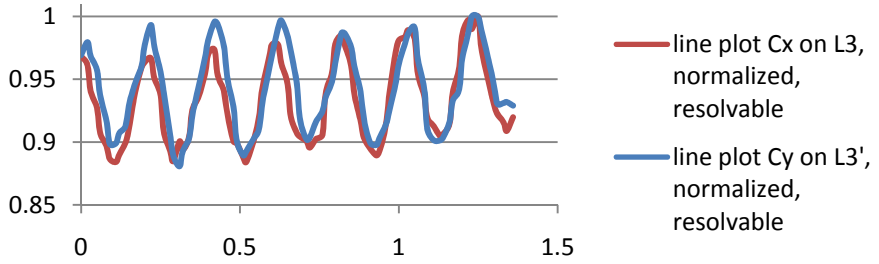

Table 4-1 (c) TXM image and the line plots at tilt angle = 20 mrad. The line plots were drawn on (i) line L1, and line L1’ in the second zone (50~60 nm), (ii) line L2, and line L2’ in the forth zone (70~80 nm), (iii) line L3, and line L3’ in the outmost zone (90~100nm).

	TXM image	Line plots
Tilt angle =30mrad	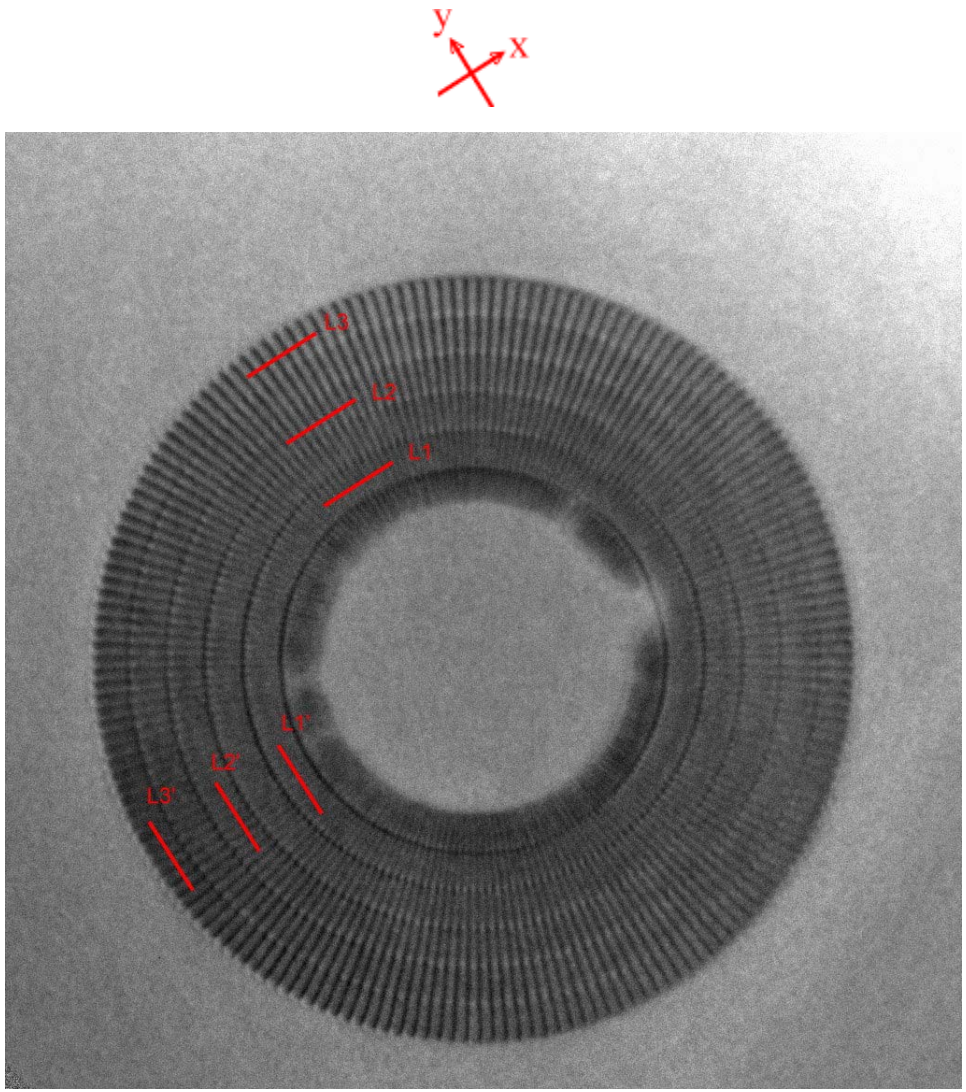	(i) 50~60 nm 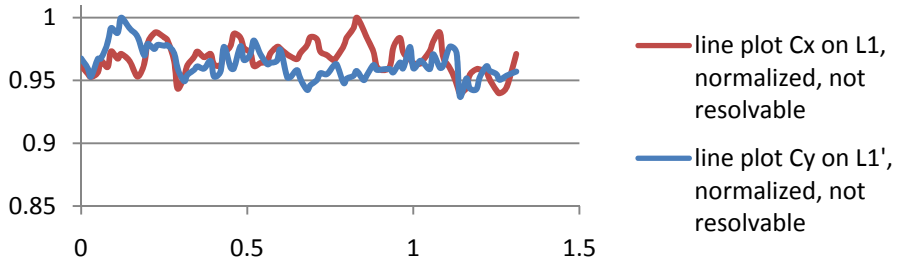 (ii) 70~80 nm 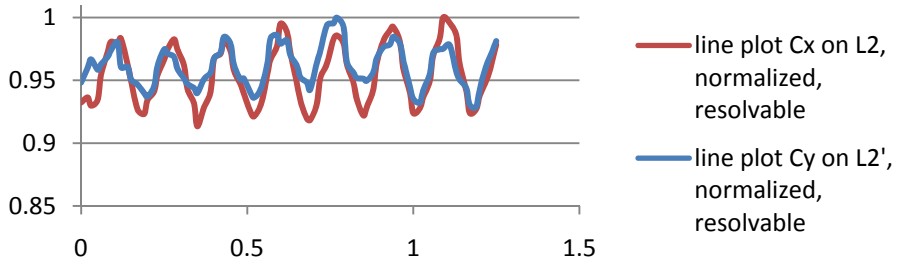 (iii) 90~100 nm 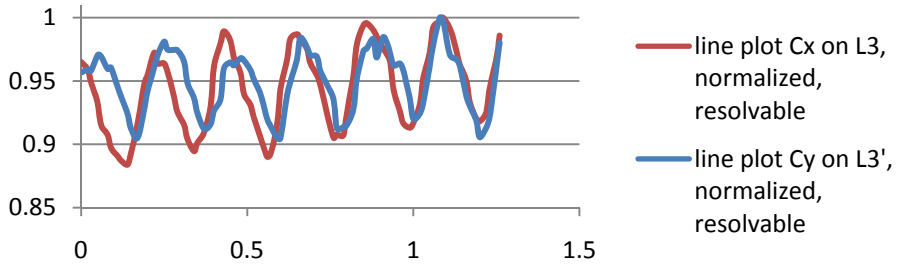

Table 4-1 (d) TXM image and the line plots at tilt angle = 30 mrad. The line plots were drawn on (i) line L1, and line L1' in the second zone (50~60 nm), (ii) line L2, and line L2' in the forth zone (70~80 nm), (iii) line L3, and line L3' in the outmost zone (90~100nm).

	TXM image	Line plots
Tilt angle =40mrad	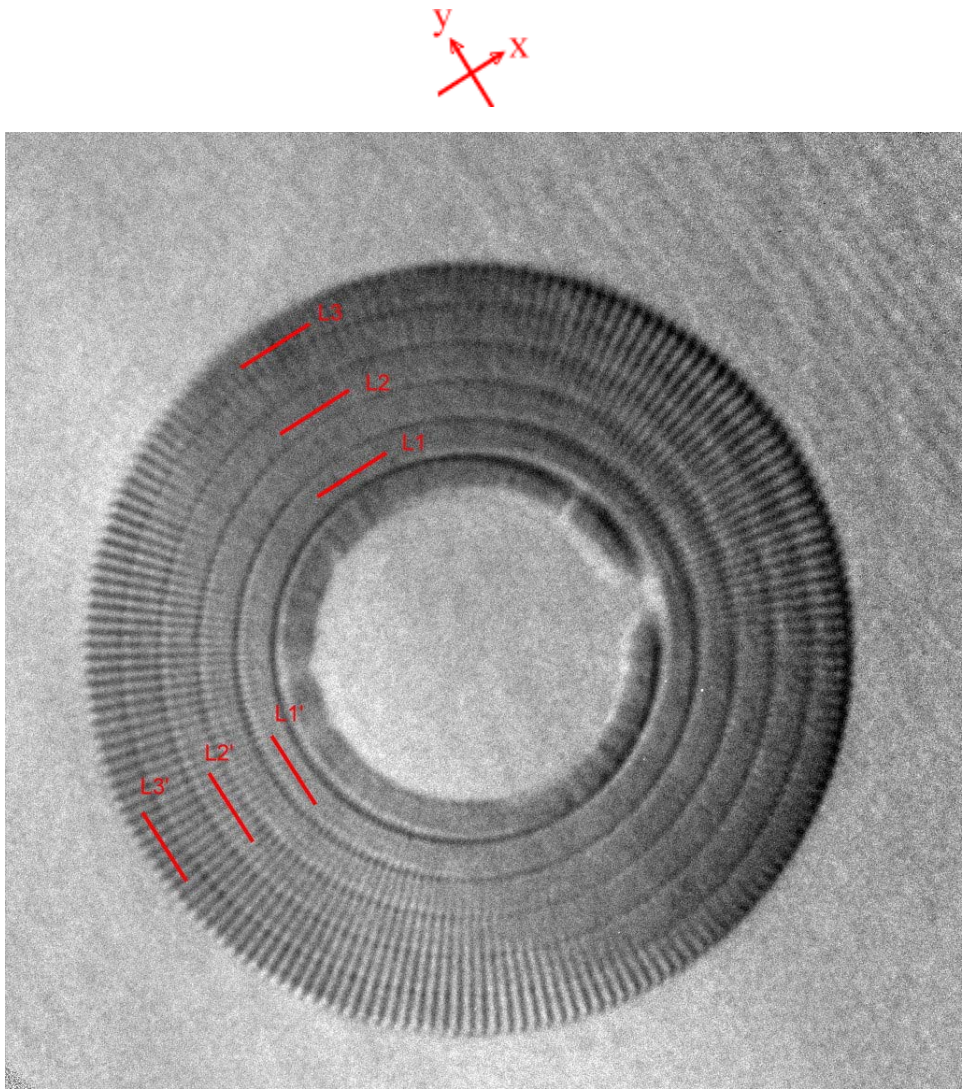	(i) 50~60 nm 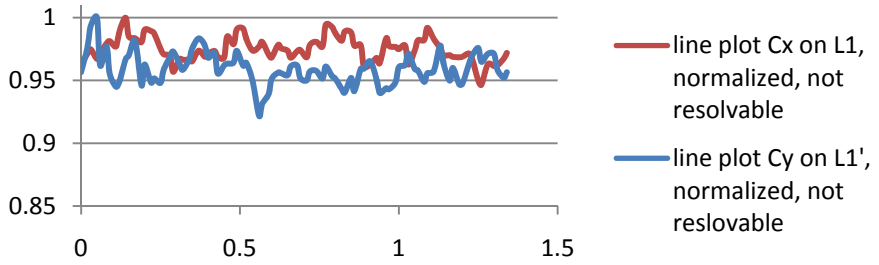 (ii) 70~80 nm 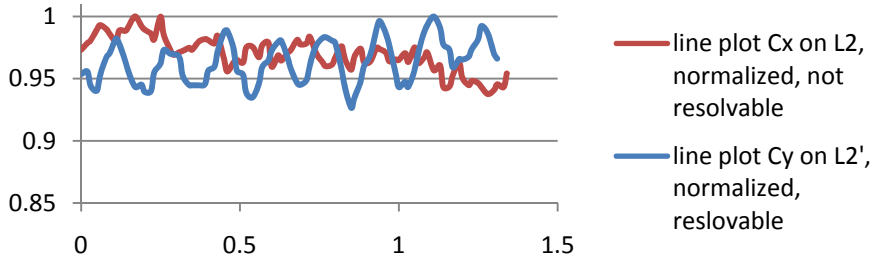 (iii) 90~100 nm 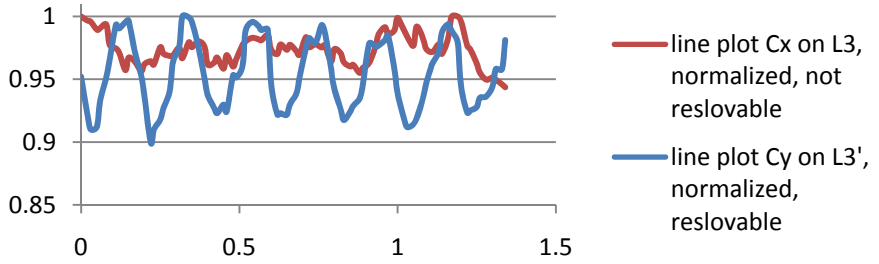

Table 4-1 (e) TXM image and the line plots at tilt angle = 40 mrad. The line plots were drawn on (i) line L1, and line L1’ in the second zone (50~60 nm), (ii) line L2, and line L2’ in the forth zone (70~80 nm), (iii) line L3, and line L3’ in the outmost zone (90~100nm).

4.3 Analysis and Summary

By the TXM images and the line plots in Table 4-1, we can see that, whether the zone plate is tilted or not, the patterns in the first and second zones are not resolvable, i.e., the resolution-limits of those TXM images are all larger than 60 nm. Briefly, the TXM image does not change a lot when the zone plate is tilted from 0 to 30 mrad., as shown in Table 4-1 (a)-(d). However, when the zone plate is tilted by 40 mrad., the TXM image becomes worse; the patterns parallel to x axis are still resolvable, but the patterns parallel to y axis become blurred (the line plots on L2, L3 at tilt angle= 40 mrad. are not periodic functions of distances, that is, the patterns which are parallel to the y axis on L2 and L3 can't be resolved when the zone plate is tilted by 40 mrad.), as show in Table 4-1 (e).

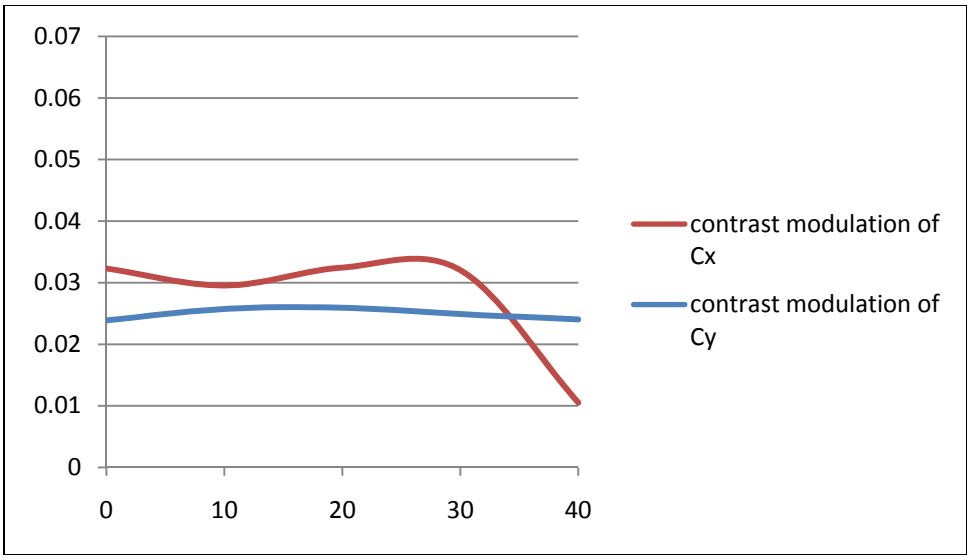

(a)

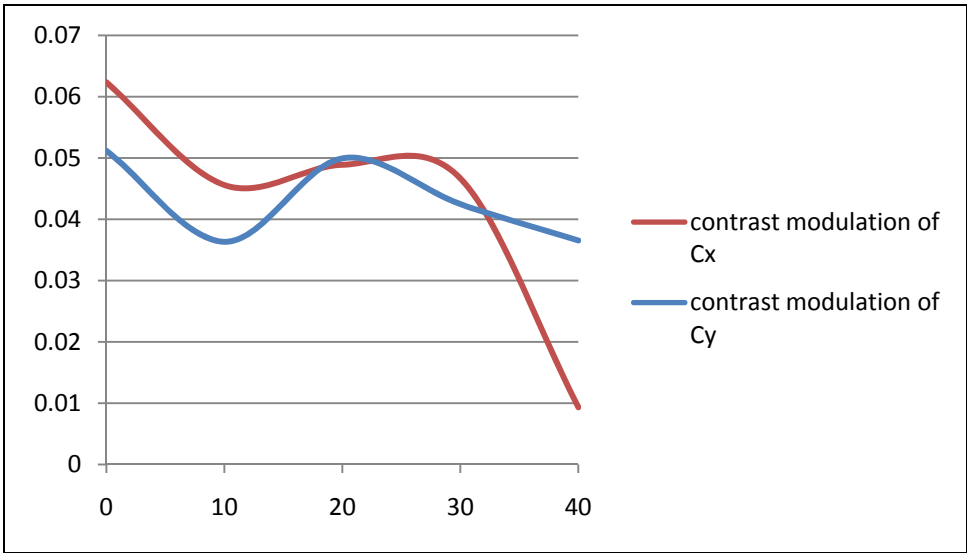

(b)

Fig. 4-3 Contrast modulation v.s tilt angle (mrad.) (a) at spatial frequency between $12.50MHz \sim 14.2857MHz \quad (\frac{1}{70nm} \sim \frac{1}{80nm})$, (b) at spatial frequency between $11.1111MHz \sim 10.0MHz \quad (\frac{1}{90nm} \sim \frac{1}{100nm})$.

In Fig. 4-3, the modulations of Cy do not change obviously as tilt angle increases (In Fig. 4-3 (a), the contrast modulation of Cy is between 0.02 and 0.03, and in Fig. 4-3 (b), it's between 0.035 and 0.052). The contrast modulations of Cx do not change a lot when the tilt angle is smaller than 30 mrad., but they decrease rapidly when the tilt angle is larger than 30 mrad.. For this reason, we say that the maximum acceptable tilt angle is 30 mrad.

Although the qualities of TXM images are affected by many reasons, and both the resolutions and contrasts of experimental results are worse than those of the simulation results, we can still see that the zone plate tilt affects the image quality.

Chapter 5
Conclusions and Future Work

5.1 Conclusions

The affections due to zone plate tilt on the TXM image can be observed in series of TXM images and their line plots in chapter 3 and 4. According to section 3.2, the focal lengths f_x and f_y in horizontal and vertical directions of a tilted zone plate are different, and the transparency is related to the optical path length in zone plate. As a result, astigmatism will occur and the quality of TXM image will be affected when the zone plate is tilted. By the simulation and experimental results, the expectance in section 3.2 is proved to be right. Zone plate tilt will make the TXM image becomes distorted and blurred, and both the simulation and experimental results indicate that the contrast of image becomes lower as the tilt angle increases. In the following section, we will discuss about what we are going to do in the future.

5.2 Future Work

Defective Zone Plates

Sometimes, the zone plate in TXM system is not perfect, since the fabrication of zone plate is not mature enough currently. In the future, we will try to calculate the transmission functions of those defective zone plates, and use the Matlab program which is introduced in chapter 3 to simulate the TXM images.

Coherence of Light Source

The light source of TXM system is partially coherent. However, we used a coherent wave function to be the light source in the simulation Matlab code. As a result, there are diffraction patterns in the simulated TXM images in chapter 3.

We tried to use many different optical waves U_{1_1}, U_{1_2}, …., U_{1_n} to be the light source, calculate the optical fields on the image plane U_{6_1}, U_{6_2}, …., U_{6_n} by the Matlab program respectively, and then sum the intensities of the wave functions. The intensity distribution function on the image plane will be:

$$I_6 = (A_1 \cdot |U_{6\_1}|^2 + A_2 \cdot |U_{6\_2}|^2 + ... + A_n \cdot |U_{6\_n}|^2) = \sum_{m=1}^{n} A_m \cdot |U_{6\_m}|^2$$

, where A_m is the weight of the mth term.

Nevertheless, it didn't get rid of all the diffraction patterns in the simulated image. So we will try to find out better solutions in the future.

Image Recovery

According to Fourier optics theory, the optical fields in TXM system can be solved, the calculation and the simulated wave distributions have been shown in section 3.1.

See Fig. 3.1, if we know the optical field U_6 at $z=z_1+z_2+z_3$ on the image plane, the distances z_2, z_3 between each component, and the effective transmission function of the zone plate, we can solve the optical field U_3 at $z=z_1^+$ behind the sample by de-convolution. And we can solve the transmission function of the sample T_{sample} by dividing U_3 by U_2.

By eq. (3.10), we know $U_6(x,y)$ is the convolution of $U_5(x,y)$ and $p_{z3}(x,y)$. If we know $U_6(x,y)$ and the distance z_3, we can solve $U_5(x,y)$ by de-convolution:

$$U_5(x,y_y) = F^{-1}\{U_5(f_x,f_y)\} = F^{-1}\{\frac{U_6(f_x,f_y)}{P_{z3}(f_x,f_y)}\} \equiv U_6(x,y) \overline{\otimes} p_{z3}(x,y) \qquad (5.1)$$

, where "$\overline{\otimes}$" denotes de-convolution, or

$$U_5(x,y_y) = F^{-1}\{U_6(f_x,f_y)\cdot P'_{z3}(f_x,f_y)\} \qquad (5.2)$$

, where $P'_{z3}(f_x,f_y) = F\{\frac{\exp(-jkz_3)}{-j\lambda z_3}\cdot\exp[-k\cdot(x^2+y^2)/2z_3]\}$.

$U_4(x,y)$ can be solved by dividing $U_5(x,y)$ by the effective transmission function of zone plate $T_{ZP}(x,y)$:

$$U_4(x,y) = \frac{U_5(x,y)}{T_{ZP}(x,y)} \qquad (5.3)$$

Similarly,

$$U_3(x,y) = F^{-1}\{\frac{U_4(f_x,f_y)}{P_{z2}(f_x,f_y)}\} = U_4(x,y) \overline{\otimes}\ p_{z2}(x,y) \tag{5.4}$$

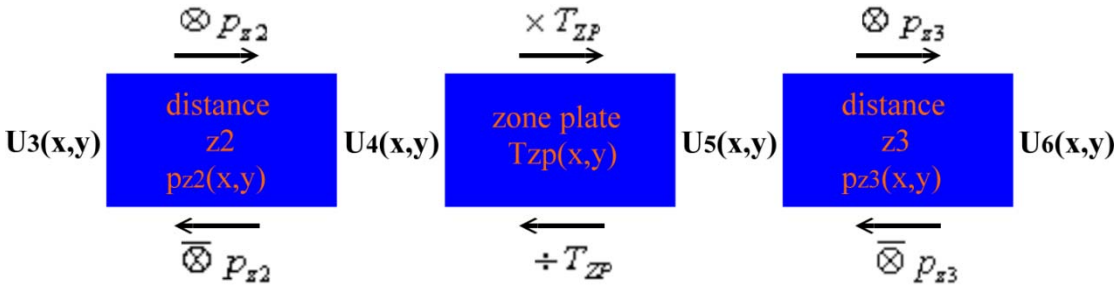

Fig. 5-1 Illustration of image recovery.

$U_3(x,y)$ is the wave function at $z=z_1^+$. If we know the wave function $U_2(x,y)$ at $z=z_1^-$, by eq.(3.6), the transmission function of the sample $T_{sample}(x,y)$ can be solved by dividing $U_3(x,y)$ by $U_2(x,y)$:

$$T_{sample}(x,y) = \frac{U_3(x,y)}{U_2(x,y)} \tag{5.5}$$

As a result, we can know how the sample looks like (recover the image), although the zone plate is tilted by using de-convolution method.

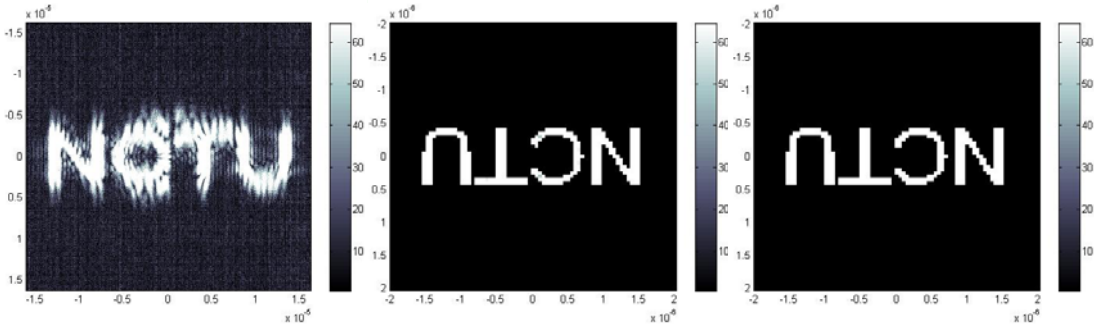

(a) (b) (c)

Fig. 5-2 (a) $|U_6|$, the simulated TXM image was obtained at tilt angle=80 mrad., (b) $|U_3|$, the wave amplitude distribution behind the sample, (c) $|T_{ZP}|$, the transparency of the sample. (b) and (c) were gotten by de-convolution method.

The de-convolution method can recover the original transparency of the sample even if the TXM image is blurred, the simulation results are shown in Fig. 5-2. We will try to recover the experimental TXM images by de-convolution method in the future.

Reference

[1] G. Yin, “Phase Imaging In Transmission xx-ray Microscope”

[2] CXRO website: http://www-cxro.lbl.gov/

[3] E. Hecht, “Optcis”

[4] J. W. Goodman, “Introduction To Fourier Optics”, chapter 4.

[5]. J. Kirz, “Phase zone plates for x rays and the extreme uv”, Journal of the optical society of America. Volume 64, number 3, March 1974.

[6] W. Chao, B. D. Harteneck, J. A. Liddle, E. H. Anderson1 & D. T. Attwood, “Soft X-ray microscopy at a spatial resolution better than 15nm”, Nature, Vol 435|30 June 2005|doi:10.1038/nature03719

[7] Y Feng, M. Feser, A. Lyon, S. Rishton, X. Zeng, S. Chen, S. Sassolini, and W. Yun, “Nanofabrication of high aspect ratio 24 nm x-ray zone plates for x-ray imaging applications”, J. Vac. Sci. Technol. B, Vol. 25, No. 6, Nov/Dec 2007

[8] G. Yin, M. Tang, Y. Song, F. Chen, F.W. Duewer, W. Yun, C. Ko, H.D. Shieh, and K. S. Liang, “Energy-tunable transmission x-ray microscope for differential contrast imaging with near 60 nm resolution tomography”, Appl. Phys. Lett. 88, 241115(2006)

[9] G. Yin, M. Tang, Y. Song, F. Chen, F.W. Duewer, W. Yun, M. Feser, H.D. Shieh, and K. S. Liang, “30 nm resolution x-ray imaging at 8 keV using third order diffraction of a zone plate lens objective in a transmission microscope”, Appl. Phys. Lett. 89, 221122(2006)

[10] Y. T. Chen, T. N. Lo, C. W. Chiu, J. Y. Wang, C. L. Wang, C. J. Liu, S. R. Wu, S. T. Jeng, C. C. Yang, J. Shiue, C. H. Chen, Y. Hwu, G. C. Yin, H. M. Lin, J. H. Jef and G. Margaritondo “Fabrication of high-aspect-ratio Fresnel zone plates by e-beam lithography and electroplating” J. Synchrotron Rad. (2008). 15, 170–175)